ERDC/ITL TR-13-4

US Army Corps
of Engineers®
Engineer Research and
Development Center

ERDC
INNOVATIVE SOLUTIONS
for a safer, better world

Bio-inspired Research Program

Towards Development of Innovative Bio-Inspired Materials by Analyzing the Hydrodynamic Properties of Polyondon Spathula (Paddlefish) Rostrum

Reena R. Patel and Guillermo A. Riveros

September 2013

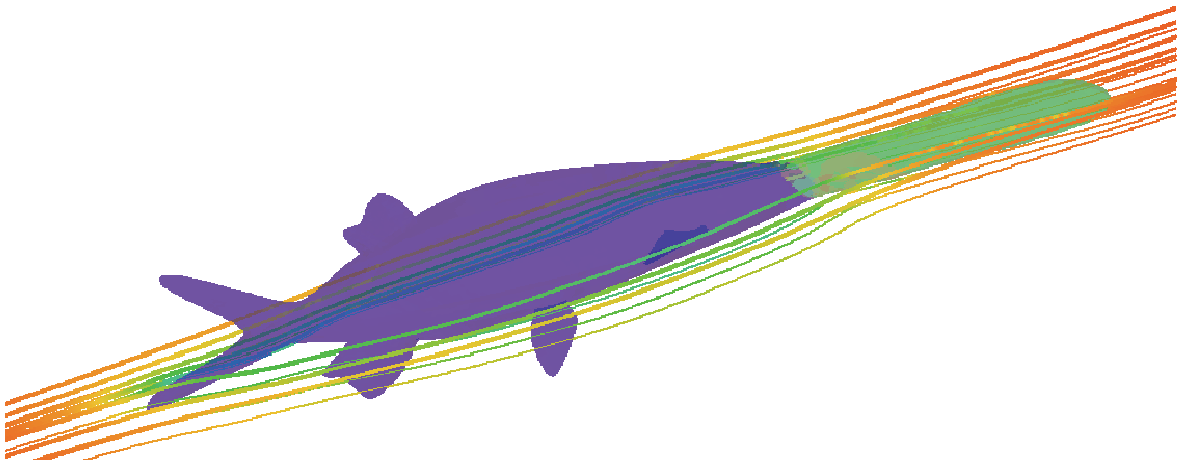

Information Technology Laboratory

The US Army Engineer Research and Development Center (ERDC) solves the nation's toughest engineering and environmental challenges. ERDC develops innovative solutions in civil and military engineering, geospatial sciences, water resources, and environmental sciences for the Army, the Department of Defense, civilian agencies, and our nation's public good. Find out more at www.erdc.usace.army.mil.

To search for other technical reports published by ERDC, visit the ERDC online library at http://acwc.sdp.sirsi.net/client/default.

Bio-inspired Research Program

ERDC/ITL TR-13-4
September 2013

Towards Development of Innovative Bio-Inspired Materials by Analyzing the Hydrodynamic Properties of Polyondon Spathula (Paddlefish) Rostrum

Reena R. Patel and Guillermo A. Riveros

Information Technology Laboratory
US Army Engineer Research and Development Center
3909 Halls Ferry Road
Vicksburg, MS 39180-6199

Final report

Prepared for US Army Corps of Engineers
Washington, DC 20314-1000

Abstract

Paddlefish can be distinguished from other freshwater fish by the presence of a long paddle shaped snout (Rostrum). The Rostrum has desirable mechanical characteristics that could be explored to design bio-inspired materials that have better strength to weight ratio. The Rostrum is large and generates lift like an aircraft wing. It acts as a stabilizer preventing drag during filter feeding when the mouth is wide open. This report will discuss the Fluid Structure Interaction simulations conducted to analyze the lift generated by the Rostrum, fluid flow around the fish, pressures on the Rostrum, fluid induced swimming enhancements, and stabilizing properties of the Rostrum. The report analyses and discusses the experimentally measured forward body velocity of Paddlefish during filter feeding. Laminar flow with different angles of attack (0, 5, and 10) along and against the direction of the longitudinal axis of the swimming fish are also studied and discussed.

Contents

Abstract ii

Figures and Tables v

Preface vii

Unit Conversion Factors viii

1 Introduction 1

1.1 Bio – inspiration 1
1.2 Paddlefish Characteristics 1
1.3 Paddlefish population decline 3
1.4 Objective 3
1.5 Fluid Structure Interaction Simulations 5

2 Fluid Structure Interaction Formulation to Study Flow around the Polyondon Spathula (Paddlefish) 6

2.1 Multiphysics Methods 6
2.2 Computational Fluid Dynamics Analysis 7
2.2.1 Numerical Implementation: 8
2.2.2 Least-square gradient approximation: 9
2.2.3 Advection methods 10
2.3 Computation Solid Mechanics Analysis 10

3 Co-Simulation CFD/CSM details 12

3.1 Analysis Details 12
3.2 CFD Model Details 13
3.3 CSM Model Details 14

4 FSI Results 18

4.1 Test Case Details 18
4.2 Simulation time and HPC information 18
4.3 Velocity profile for fish swimming against the flow direction 19
4.4 Velocity profile for fish swimming along the flow direction 21
4.5 Pressure profile for fish swimming against the flow direction 23
4.6 Pressure profile for fish swimming along the flow direction 25
4.7 Pressure graph near mouth of fish for the three angles of attack 27
4.8 Pressure on fins of the Paddlefish 27
4.9 Pressure graph on bottom/top surface of Rostrum 28
4.10 Velocity graph at Rostrum tip (1) 32
4.11 Velocity graph at Rostrum tip (2) 32
4.12 Streamlines depicting flow patterns 34

5 Conclusions and Recommendations 36

5.1 Conclusions....36
5.2 Velocity of fish....36
5.3 Pressure on Rostrum....37
5.4 Angle of attack of Rostrum....37
5.5 Recommendations for Further Research....37

References....39

Report Documentation Page

Figures and Tables

Figures

Figure 1. Stellate bone of Rostrum (Hoover 2013). 2
Figure 2. Rostrum Injuries (Hoover 2013). 3
Figure 3. Paddlefish population distribution (Jennings and Zigler 2009). 4
Figure 4. Bio-inspiration flowchart. 5
Figure 5. Flowchart of the incompressible CFD fluid solver. 9
Figure 6. Flowchart of explicit structure solver. 11
Figure 7. Partitioned fluid-structure interaction. 13
Figure 8. CFD model dimensions. 13
Figure 9. Experimental Nano-indentation data (Hoover 2013). 14
Figure 10. Cross-sections of Rostrum. 15
Figure 11. Fish body used in CSM. 16
Figure 12. Rostrum dimensions. 16
Figure 13. Rostrum structure model dimensions by Hoover (2013). 17
Figure 14. Rostrum structure model dimensions by Hoover (2013). 17
Figure 15. Diamond. SGI ALtix Ice – 172 TFLOPS. 19
Figure 16. Velocity profile for fish moving against the flow direction at an angle of attack of 0 degrees. 20
Figure 17. Velocity profile for fish moving against the flow direction at an angle of attack of 5 degrees. 20
Figure 18. Velocity profile for fish moving against the flow direction at an angle of attack of 10 degrees. 21
Figure 19. Velocity profile for fish moving along the flow direction at an angle of attack of 0 degrees. 21
Figure 20. Velocity profile for fish moving along the flow direction at an angle of attack of 5 degrees. 22
Figure 21. Velocity profile for fish moving along the flow direction at an angle of attack of 10 degrees. 22
Figure 22. Pressure profile for fish moving against the flow direction at an angle of attack of 0 degrees. 23
Figure 23. Pressure profile for fish moving against the flow direction at an angle of attack of 5 degrees. 24
Figure 24. Pressure profile for fish moving against the flow direction at an angle of attack of 10 degrees. 24
Figure 25. Pressure profile for fish moving along the flow direction at an angle of attack of 0 degrees. 25
Figure 26. Pressure profile for fish moving along the flow direction at an angle of attack of 5 degrees. 26

Figure 27. Pressure profile for fish moving along the flow direction at an angle of attack of 10 degrees. 26
Figure 28. Pressure near the mouth of fish for the three angles of attack. 27
Figure 29. Pressure reference point near the mouth of fish for the three angles of attack. 28
Figure 30. Reference point on fins 1, 2, 3, and 4. 28
Figure 31. Pressure on fins 1 and 2. 29
Figure 32. Pressure on fins 3 and 4. 29
Figure 33. Path reference on Rostrum top. 30
Figure 34. Path reference on Rostrum bottom. 30
Figure 35. Pressure as a function of true distance on Rostrum top & bottom at an angle of attack of 10 degrees. 31
Figure 36. Pressure as a function of true distance on Rostrum top & bottom at an angle of attack of 5 degrees. 31
Figure 37. Pressure as a function of true distance on Rostrum top & bottom at an angle of attack of 0 degrees. 32
Figure 38. Velocity reference point at Rostrum tip (1) 33
Figure 39. Velocity as a function of time at Rostrum tip (1) 33
Figure 40. Velocity reference point at Rostrum tip (2) 34
Figure 41. Velocity as a function of time at Rostrum tip (2) 34
Figure 42. Streamlines when fish is moving against the flow direction 35
Figure 43. Streamlines when fish is moving in the flow direction 35

Tables

Table 1. Application-based comparison of Multiphysics methods. 7
Table 2. Average result for Modulus from force-displacement curves. 15
Table 3. Test Case Velocities. 18

Preface

This study was conducted for the Material Modeling for Force Protection project under Project MR003D, "(Paddlefish) Bio-structural Analysis and Modeling (6.1) project," WIC 1DDC3A. The technical monitor was Dr. Ed Perkings.

The work was performed by Reena R. Patel and Dr. Guillermo A. Riveros of the Computational Analysis Branch of the Computational Science and Engineering Division, US Army Engineer Research and Development Center, Information Technology Laboratory. At the time of publication, Elias Arredondo was Chief, CEERD-IE-C; Dr. Robert Wallace was Chief, CEERD-IE; and David R. Richards, CEERD-IV-T was the Technical Director for Engineering and Science. The Deputy Director of ERDC-ITL was Patti Duett and the Director was Dr. Reed Mosher.

COL Jeffrey R. Eckstein was the Commander of ERDC, and Dr. Jeffery P. Holland was the Director.

Unit Conversion Factors

Multiply	By	To Obtain
cubic inches	1.6387064 E-05	cubic meters
inches	0.0254	meters
pounds (force)	4.448222	newtons
pounds (force) per foot	14.59390	newtons per meter
pounds (force) per inch	175.1268	newtons per meter
pounds (force) per square inch	6.894757	kilopascals
pounds (mass)	0.45359237	kilograms
pounds (mass) per cubic foot	16.01846	kilograms per cubic meter
pounds (mass) per cubic inch	2.757990 E+04	kilograms per cubic meter
pounds (mass) per square foot	4.882428	kilograms per square meter
pounds (mass) per square yard	0.542492	kilograms per square meter
slugs	14.59390	kilograms
square inches	6.4516 E-04	square meters

1 Introduction

1.1 Bio–inspiration

Nature has evolved from a single cell to complex biomechanics. Several novel materials with superior properties already exist in nature. For example, the woodpecker's head has been a source of inspiration for designing shock absorbers. Silk from silkworms and orb-weaving spiders have been studied to incorporate their desirable mechanical properties for use in biomaterials (Vepari and Kaplan 2007). One property that distinguishes the naturally occurring materials from man-made materials is the unique hierarchical structure. It is the presence of this hierarchical structure that imparts these materials their superior strength and performance capability. In comparison to man-made materials, naturally occurring materials have a very limited number of basic components. Advancement towards hierarchical structure gives them their uniqueness, which enables them to withstand adversity, adapt, and heal. Looking at nature from an engineer's eye and reverse engineering the reason for the development of the unique hierarchical structure may lead us towards designing materials that have broader use limits and areas (Sen 2011).

1.2 Paddlefish Characteristics

The Rostrum of Paddlefish is a unique structure comprising of a network of cartilage, tissue, and interlocking star shaped bones called stellate bones. Figure 1 shows the stellate bone arrangement in the Rostrum of Paddlefish. The Rostrum imparts sensory, electro and tactile (Hoover 2013), hydrodynamics and strength properties depending on the age of the fish. Paddlefish are known to feed efficiently in both laminar and turbulent flows. The sensory functions of the Rostrum enable them to detect the type of flow (Gurgens at al. 2000). Also, the sensory functions allow them to detect tiny zooplankton by detecting them void of sight (Wilkens et al. 1997). Furthermore, Paddlefish readily try to feed on dipoles that emitt electrical signals (Wilkens and Hofmann 2007). Paddlefish swim with their mouth wide open during filter feeding and take in enormous amounts of water. The gill rakers help them filter the tiny zooplankton from the water. During filter feeding, Paddlefish swim faster. The forward body velocity is used to transport the water at high speed and filter food quickly and efficiently. The function of the Rostrum changes at different stages of the life of Paddlefish.

Figure 1. Stellate bone of Rostrum (Hoover 2013).

In juvenile stage, the shape of the Rostrum is linear and size and area of the Rostrum is almost one-third the body length. The primary function of the Rostrum at juvenile stage is sensory. During the sub-adult stage the shape of the Rostrum is spatulate and the primary function of the Rostrum is hydrodynamic. During this stage, the Paddlefish are active filter feeders. In the adult stage, the shape of the Rostrum is linear and the primary function is mechanical. Early researchers thought the Rostrum was used to dig for food (Forbes 1878, 1888a, and 1888b; Jordan and Evermann 1896; Stockard 1907; Alexander 1914) or dislodge organisms from vegetation (Norris 1923; Beach 1902). This notion was put aside when Paddlefish were found to be filter feeders (Sprague 1929; Meyer 1960). Adult Paddlefish can survive without Rostrum, but they feed less efficiently and are comparatively thinner. Figure 2 shows a Paddlefish with Rostrum injuries (Hoover 2013) Paddlefish are extremely mobile species. They have been known to travel more than 2000 miles in river systems. The size, shape, and position of the Rostrum help generate lift as in a journal article written by Allen and Riveros (2013), currently in review. During filter feeding, the added weight of the enormous amount of water would pose stability issues in absence of the lift generated by the Rostrum.

Figure 2. Rostrum Injuries (Hoover 2013).

1.3 Paddlefish population decline

Paddlefish are among the most endangered groups of fishes in North America. They were once abundant in most central US river systems. Figure 3 shows the population data of Paddlefish (Jennings and Zigler 2009). One of the main reasons for their population decline is overharvesting (Williamson 2003). They are commercially exploited for their eggs, or roe (caviar) (Tower 1908; Stockard 1908; and Saffron 2002). Additionally, sedimentation and river modifications are other reasons for their population decline. One of the objectives of this research is to create awareness about this unique fish and learn from the structural and mechanical behavior of the Rostrum to design novel bio-inspired material that would have better strength to weight ratio. These bio-inspired materials could have potential uses in the area of body and vehicle armor, ship designs, blast loading energy dissipation, repairs of fatigue and fracture in navigation steel structures, among others.

1.4 Objective

Understanding the dynamic effects, forces, and pressures involved in a swimming fish will enhance the knowledge in various applied engineering fields, i.e. designing submarines, ships, body armors etc. Bergmann and Iollo (2011) have studied the flow and vortex shedding in 2D and 3D fish like objects that resemble an airfoil. Their study focuses on the power required by the fish for swimming, both for a single fish and for small fish schools. The present study follows the experimental work done by Sanderson et al. (1994) where the buccal flow velocity of the Paddlefish is measured during ram ventilation, ram suspension feeding, and prey

processing. This work has measured the forward body velocities of Paddlefish kept in stagnant water so that the velocity they measure is the body velocity of fish and not the water. The simulations carried out in the present study are done at the Reynolds number 30, proportional to velocities in laminar flow regime and have been used for model validation.

Figure 3. Paddlefish population distribution (Jennings and Zigler 2009).

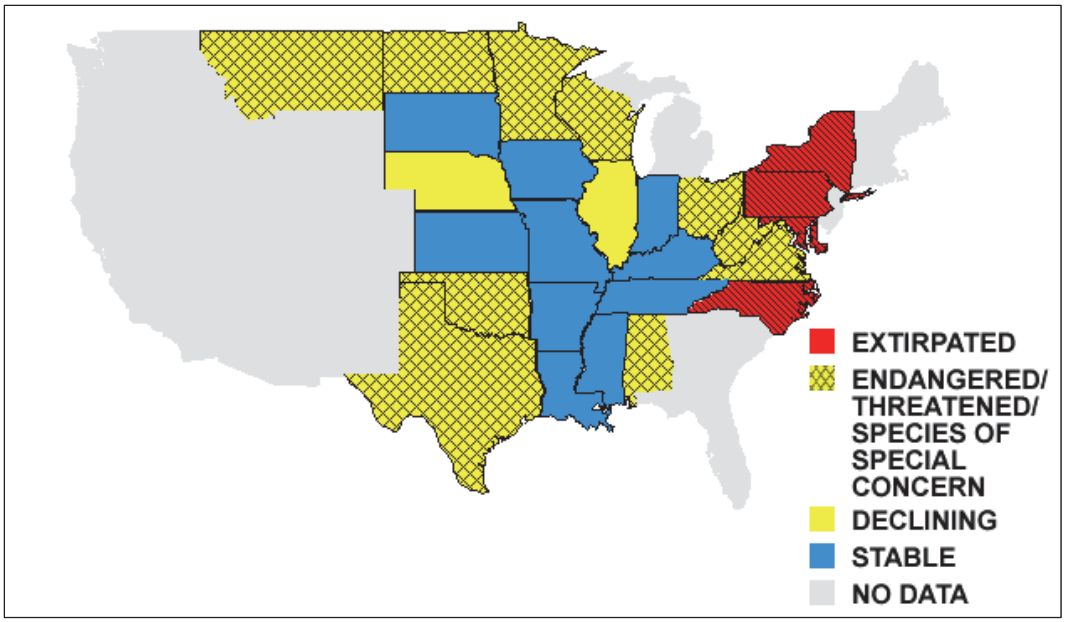

Figure 4 shows a pictorial representation of the flowchart depicting the process of application of this research. It shows the process involved in designing novel high performance materials. The end product of such cycle could be a material that has better strength to weight ratio and could be used to make lightweight, high performance body armor for our soldiers.

The objective of this study can be classified as follows:

1. Conduct fluid structure interaction simulation,
2. Study the effect of flow and fish velocity on the Rostrum,
3. Observe the pressure distribution on the top and bottom surface of the Rostrum, and
4. Analyze the effect of angle of attack on the uplift pressure and flow velocity.

1.5 Fluid Structure Interaction Simulations

The recent advancements of computing power have had a remarkable influence on the nature of simulations being carried out on high performance computers. Complicated phenomenon like the interaction of one or more solid structure with the surrounding fluid can be carried out with the use of sophisticated well-tested algorithms. The effect of sub-merged solid structure on the flow pattern can be studied in great detail with the use of Multiphysics techniques like the fluid structure interaction (FSI). Six test cases are simulated for the present study. Laminar flow with different angles of attack (0, 5, and 10) and velocities of the swimming fish are studied and discussed. The report discusses the lift generated by the Rostrum, fluid flow patterns around the fish body, pressures on the Rostrum, fluid induced swimming enhancements, and stabilizing properties of the Rostrum.

Figure 4. Bio-inspiration flowchart.

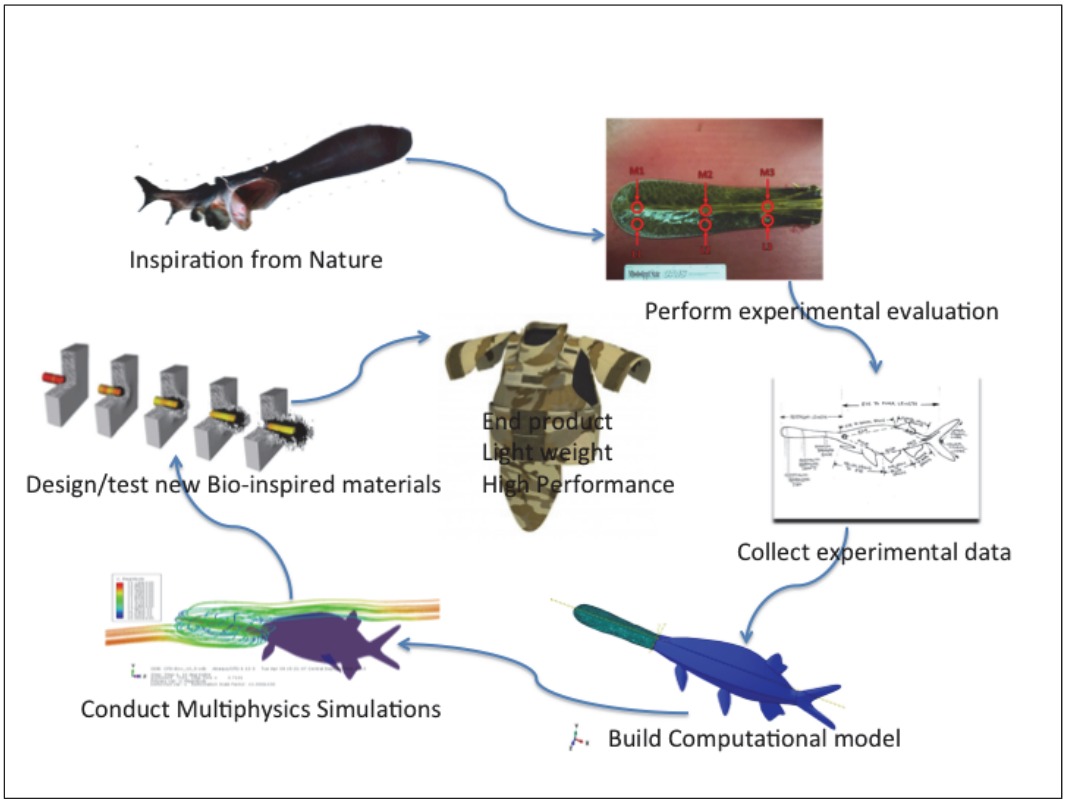

2 Fluid Structure Interaction Formulation to Study Flow around the Polyondon Spathula (Paddlefish)

2.1 Multiphysics Methods

A wide range of interdisciplinary problems can be approached using fluid structure interaction (FSI). With the recent advancement of computer power, a variety of application areas can be addressed. FSI is a Multiphysics, non-linear problem that involves the interaction between incompressible fluid flows and immersed flexible or rigid body structures (Hou et al. 2011). FSI problems analyze the interaction of one or more solid structures with the surrounding fluid flow. FSI problems can be solved with two approaches; monolithic and partitioned. In monolithic approach, the fluid and structure dynamics are treated in a single mathematical framework. A single system equation is formed for the whole problem. The drawback to using monolithic approach is the amount of effort that goes into developing specialized code and also the amount of labor needed to maintain such specialized code. The partitioned approach treats the fluid and structure model separately in different mathematical framework as the name suggests. Existing state of the art solvers are used to address the fluid and structure model. Data were exchanged between the fluid and structure solvers at the interface boundary. Although this approach has the advantage of using the existing legacy codes, keeping up with the interface boundary which changes in time is a challenge. Partitioned approach is used in the present study.

The present study uses Abaqus to carry out the FSI simulations. Various application-based approaches are available to address Multiphysics problems (Table 1). Multiphysics approaches with abbreviations are listed below:

- (CEL) Coupled Eulerian-Lagrangian analysis,
- (SPH) Smoothed Particle Hydrodynamics, and
- (CFD/FSI) Coupling between fluid and structure model.

FSI methods have been used for coupled fluid structure interaction problems in biomechanics applications where biofluids such as blood interacts with biological structures such as arterial walls (Prasad et al. 2011).

Table 1. Application-based comparison of Multiphysics methods.

	CEL	SPH	CFD(FSI)
Dam break	✓		
Blast loading, UNDEX	✓	✓	
Impact and penetration (Element conversion)		✓	
Heat Transfer	✓		✓
Incompressible fluid flow around deformable structures	✓		✓

2.2 Computational Fluid Dynamics (CFD) Analysis

The integral form of the momentum equation for an arbitrary control volume can be written as the following:

$$\frac{d}{dt}\int_{Vol}\rho V\,dV+\int_{S}\rho V\otimes V\cdot n dS=-\int_{Vol}\nabla p dV+\int_{S}\tau\cdot n dS+\int_{Vol}f dV \tag{1}$$

where:

Vol = arbitrary control volume with surface area S,
n = outward normal to S,
ρ = density of fluid,
V = velocity vector,
$V\otimes V$ = tensor product of velocity vectors,

$$V\otimes V=\begin{matrix}u^2 & uv & uw\\ vu & v^2 & vw\\ wu & wv & w^2\end{matrix} \tag{2}$$

(u, v, w) = components of velocity in (x, y, z) directions,
F = body force, and
τ = viscous shear stress.

Since the flow is incompressible,

$$\nabla\cdot \mathrm{V}=0 \tag{3}$$

Rewriting the governing equations in terms of the primitive or physical variables ρ,u,v,w, and p, we have

$$\rho\left(\frac{\partial u}{\partial t}+u\frac{\partial u}{\partial x}+v\frac{\partial u}{\partial y}+w\frac{\partial u}{\partial z}\right)=-\frac{\partial p}{\partial x}+\mu\left(\frac{\partial^2 u}{\partial x^2}+\frac{\partial^2 u}{\partial y^2}+\frac{\partial^2 u}{\partial z^2}\right)+\rho g_x \quad (4)$$

$$\rho\left(\frac{\partial v}{\partial t}+u\frac{\partial v}{\partial x}+v\frac{\partial v}{\partial y}+w\frac{\partial v}{\partial z}\right)=-\frac{\partial p}{\partial y}+\mu\left(\frac{\partial^2 v}{\partial x^2}+\frac{\partial^2 v}{\partial y^2}+\frac{\partial^2 v}{\partial z^2}\right)+\rho g_y \quad (5)$$

$$\rho\left(\frac{\partial w}{\partial t}+u\frac{\partial w}{\partial x}+v\frac{\partial w}{\partial y}+w\frac{\partial w}{\partial z}\right)=-\frac{\partial p}{\partial z}+\mu\left(\frac{\partial^2 w}{\partial x^2}+\frac{\partial^2 w}{\partial y^2}+\frac{\partial^2 w}{\partial z^2}\right)+\rho g_z \quad (6)$$

Gravity has been taken into consideration as a body force (Toro 1999).The continuity equation, after taking the incompressibility into account, reduces to the following form,

$$\frac{\partial u}{\partial x}+\frac{\partial v}{\partial y}+\frac{\partial w}{\partial z}=0 \quad (7)$$

We have four equations (4, 5, 6, and 7) and four unknowns namely *u,v,w,* and *p*. We have a closed system of equations that can be numerically solved for the unknown variables.

2.2.1 Numerical Implementation:

Figure 5 shows the flowchart of the incompressible fluid solver. The divergence free velocity condition imposed because of incompressibility makes the numerical solution of Navier-Stokes Equation a challenge. To overcome this, projection method is used. Projection method divides the velocity field into divergence free (solenoidal) and curl free (irrotational) components using Helmholtz decomposition. The projection algorithm divides the computation of velocity in two stages. In the first stage, an intermediate velocity that does not satisfy the incompressibility constraint is calculated. In the second stage, pressure is used to project the intermediate velocity onto a space of a divergence free velocity field to obtain the updated values of pressure and velocity. Hence,

$$u=u_{sol}+u_{irrot}=u_{sol}+\nabla\phi \quad (8)$$

Figure 5. Flowchart of the incompressible CFD fluid solver.

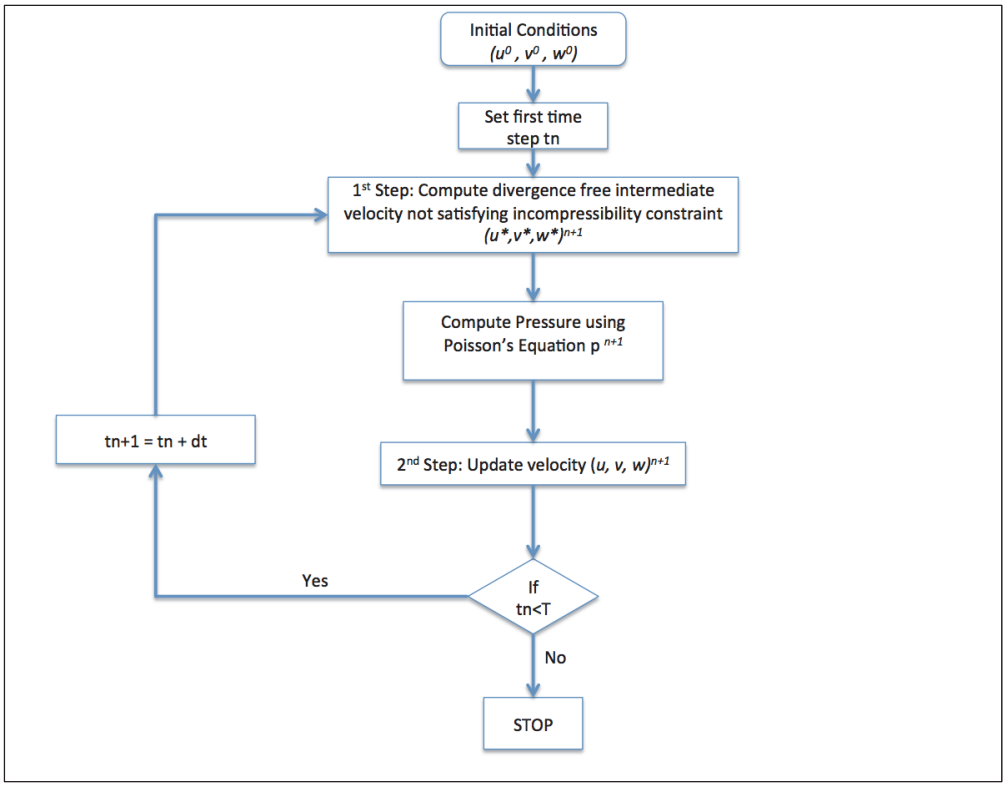

Since, $\nabla \times \nabla\phi = 0$ for some scalar functions (ϕ), the divergence of the equation results in the following:

$$\nabla \cdot u = \nabla^2 \phi \tag{9}$$

Since,

$$\nabla \cdot u_{sol} = 0 \tag{10}$$

This is a Poisson equation for the scalar function(ϕ). If the vector field $\boldsymbol{u}$ is known, the above equation can be solved for the scalar function(ϕ) and the divergence part of $\boldsymbol{u}$ can be obtained from the following relation:

$$u_{sol} = u - \nabla \phi \tag{11}$$

2.2.2 Least-square gradient approximation:

The discretization of viscous terms requires gradient of primitive variables across the cell interfaces. The solution method uses a linearly complete second order accurate least-square gradient estimation. This facilitates

accurate computation of dual edge fluxes for both advective and diffusive processes.

2.2.3 Advection methods

The solver uses edge-based treatment for advection terms. It preserves the smooth variation to 2nd order in space. The advection algorithm uses least-square gradient approximation with topologically independent slope limiters. Sharp gradient are captured within approximately 2-3 finite elements. The solver uses the slope limiters in addition to the local diffusive limiter thereby preventing over/under shoots in advected fields

2.3 Computation Solid Mechanics Analysis

The explicit dynamic analysis procedure uses explicit integration rule coupled with the use of diagonal "lumped" element mass matrices. Explicit central difference integration rule is used to integrate the equation of motion of the body.

$$\dot{U}^{(i+\frac{1}{2})} = \dot{U}^{(i-\frac{1}{2})} + \frac{\triangle t^{(i+1)} + \triangle t^{(i)}}{2} \ddot{U}^{(i)} \tag{12}$$

$$U^{(i+1)} = U^{(i)} + \triangle t^{(i+1)} \dot{U}^{(i+\frac{1}{2})} \tag{13}$$

where $\dot{U}$ is the velocity and $\ddot{U}$ is the acceleration. The computational efficiency associated with the central difference procedure is because of the use of diagonal element mass matrices. The inversion of the mass matrix used for computing accelerations is triaxial.

$$\ddot{U}^{(i)} = M^{-1} \cdot \left(F^{(i)} - I^{(i)} \right) \tag{14}$$

where M is the diagonal lumped mass matrix, F is the applied load vector. And I is the internal force vector. The explicit procedure does not need iterations and tangent stiffness matrix.

Special attention has to be given to the manner in which mean velocities are handled for the initial condition. For presenting results, the state velocities are stored as a linear interpolation of the mean velocities. Figure 6 shows the flowchart of the numerical implementation of the solver (Schutte et al. 2010).

Figure 6. Flowchart of explicit structure solver.

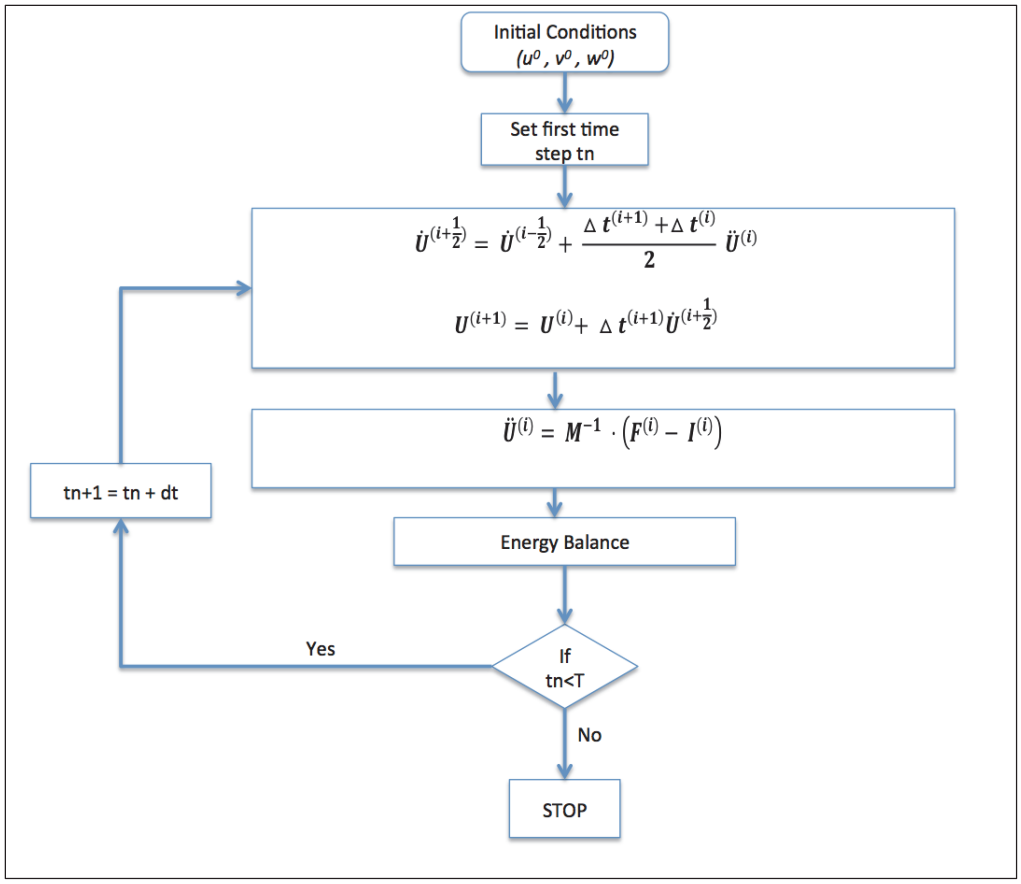

3 Co-Simulation CFD/CSM details

3.1 Analysis Details

Several methods are available to carry out Multiphysics simulations i.e. Coupled Eulerian Lagrangian (CEL), Smoothed Particle Hydrodynamics (SPH), and Fluid Structure Interaction (FSI). SPH methods are best suited for applications that involve extreme deformation (damage models and particle movements) like a blast loading. CEL methods are best suited for applications like dam break, which involves the interaction between deformable structures with compressible multiphase flows. For applications that involve the interaction of fully immersed solid deformable body with the surrounding incompressible fluid, FSI methods are well suited. Based on the application in this study, FSI method was selected. Partitioned approach is used for the fluid structure interaction analysis. The equations governing the fluid flow and displacement of structure are solved separately. The application exchanges data (Boundary conditions), each after converged iteration. The exchange of data takes place at the fluid structure interaction boundary. Rostrum is selected for exchanging data between the two solvers since it is a deformable body and the structural mechanical response to the fluid flow is of interest in this study. Additionally, there is experimental material data available for the Rostrum (Allison at al. 2013). The analysis considers the fish body as a display body. By setting the fish body as a display body, we are reducing the amount of calculations done on the structure solver and capturing the effects of the body on the flow surrounding the fish. CFD solver considers the body of the fish for simulating the flow. The structure model does computations only on the Rostrum.

Figure 7 shows a pictorial representation of the implementation of the native FSI capability for the present study. Stabilized segregated approach is used in which the structure and fluid equations are solved independently. The interface loads and boundary conditions are exchanged between the solvers after a converged increment. The co-simulation engine handles all the interaction of loads and boundary conditions between the time dependent fluid and structure domain without any user intervention.

Figure 7. Partitioned fluid-structure interaction.

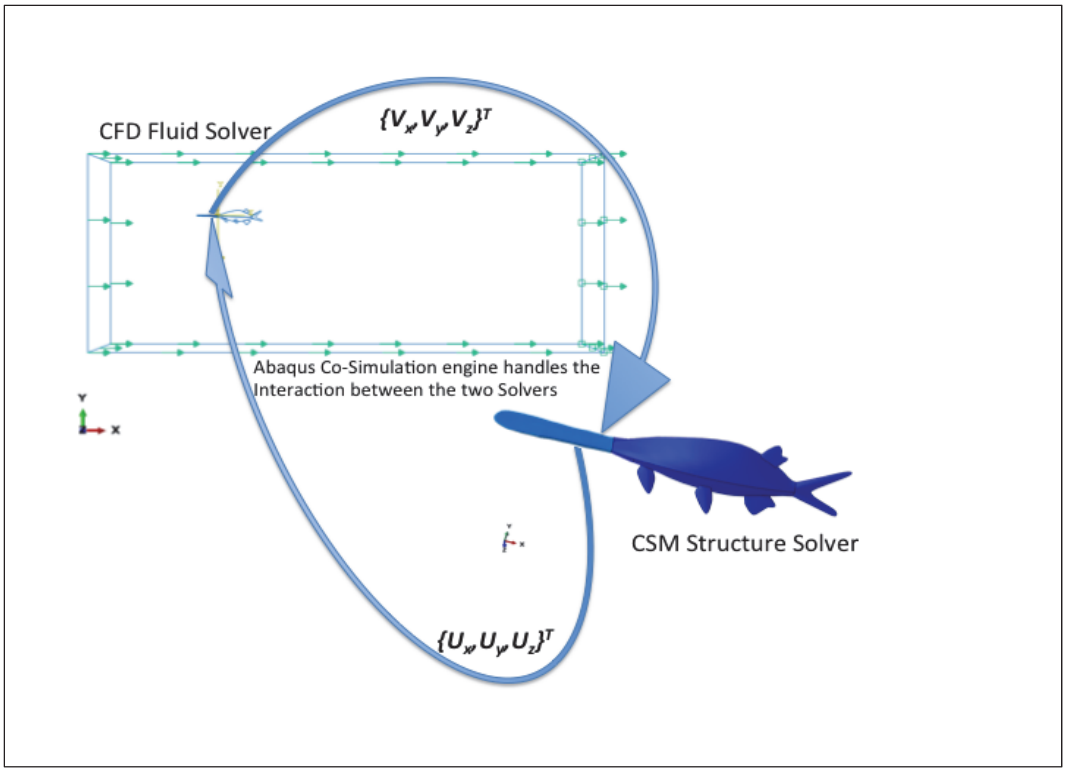

3.2 CFD Model Details

The CFD model is comprised of 123506 linear tetrahedral elements and 24071 nodes. The total number of variables in the CFD model is 72213. Figure 8 shows the dimensions of the CFD model used for the simulations.

Figure 8. CFD model dimensions.

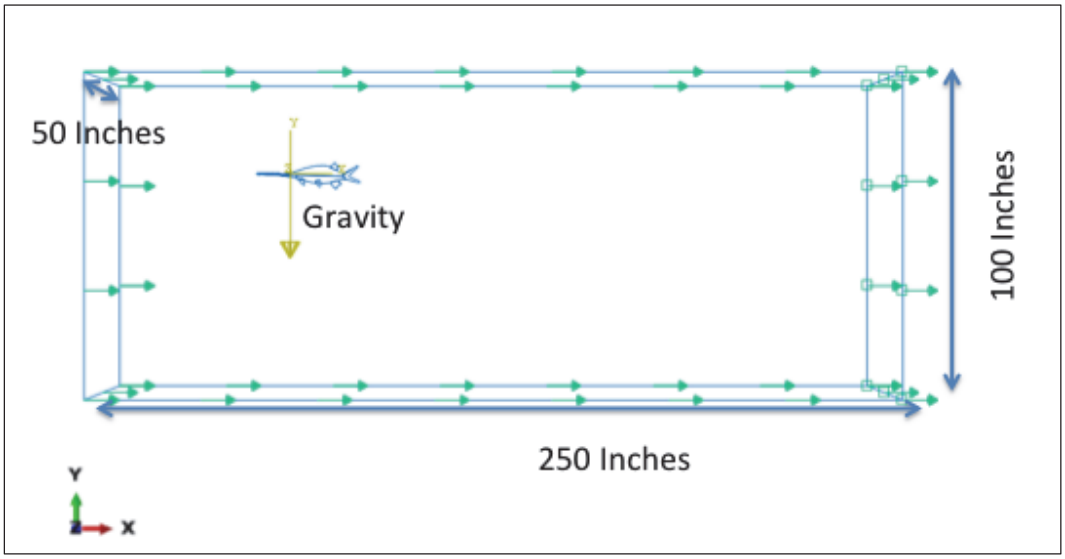

As seen in Figure 8, the CFD box is 250 inches long, 100 inches deep, and 50 inches wide. The geometry of the fish is cut out from the geometry of the fluid box by using a Boolean operation on the two geometries in Abaqus. The fish is placed at approximately 25 inches in depth and 50 inches away from the inflow. The boundary conditions are discussed in chapter 4.

3.3 CSM Model Details

Material properties used for the Rostrum are taken from the experimental data collected by Allison et al. (2013) and Mississippi State University. Nano-indentation was carried out on the Rostrum at several locations as shown in Figure 9. Modulus was calculated using the force-displacement curves. The material properties used for the simulations are taken from the values shown in Table 2. The Rostrum was partitioned at approximate locations where the data were collected. Six material properties are used for the Rostrum based on these experimental values. Looking at Figures 9, 10, and Table 2, the material properties for the middle-section M1, is higher compared to M2. Figure 10 shows the cross-section of the Rostrum from the fish mouth to its tip. Herein, M1 corresponds to slides 12 through 14 and M2 corresponds to slides 6 through 8. M1 has more compact cartilage arrangement making M1 stiffer than M2. Similarly, M3 corresponds to slides 3 through 5 in Figure 10. M3 is stiffer because of the stellate arrangement of bones as seen in Figure 1.

Figure 9. Experimental Nano-indentation data (Hoover 2013).

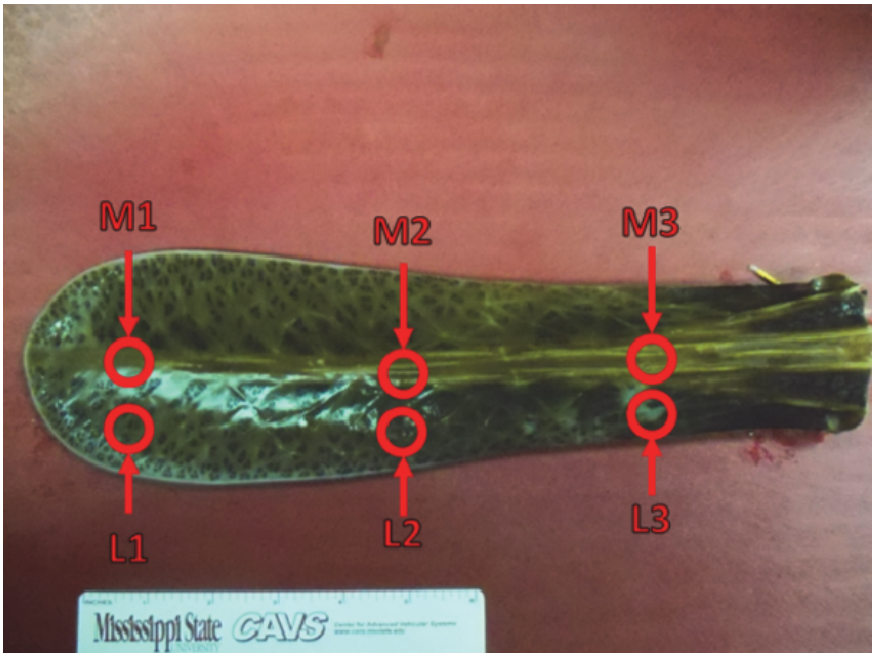

Figure 10. Cross-sections of Rostrum.

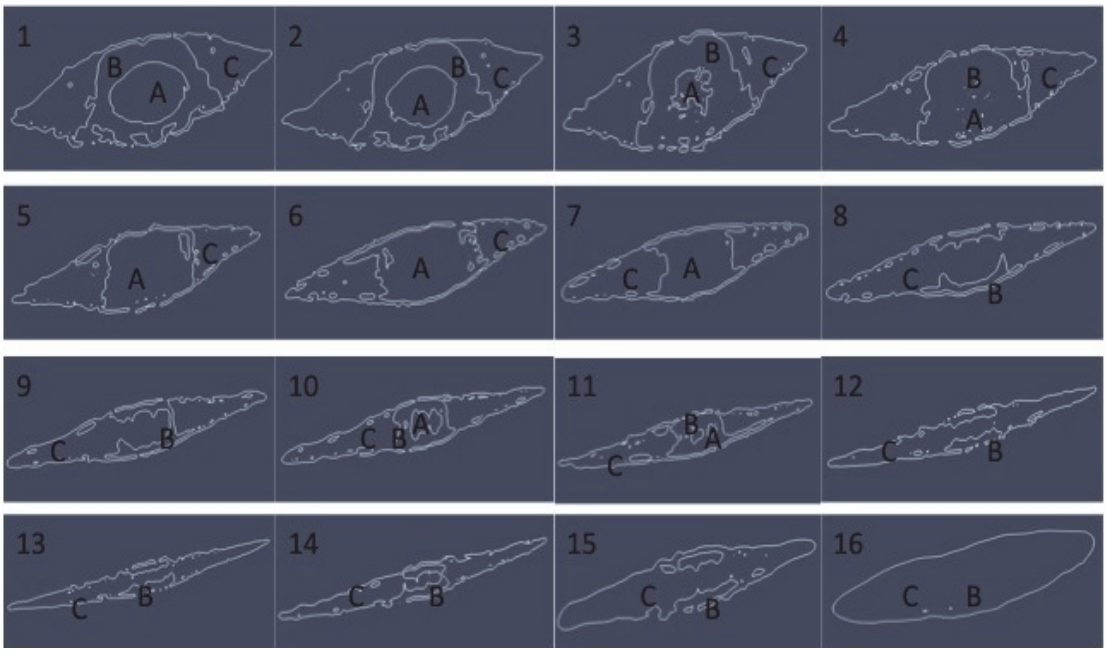

Table 2. Average result for Modulus from force-displacement curves.

	Left Side (Gpa)	Middle Section (Gpa)
1	12.48 ± 0.80	9.22 ± 0.7
2	11.50 ± 0.50	7.91 ± 0.34
3	12.16 ± 0.21	13.67 ± 0.48

The geometry of Rostrum is created from the point cloud data of the Rostrum of an adult Paddlefish. 3DMAX was used to extract a coarser STL file from the point cloud data. Solidworks was used to extract the simplified geometry in IGES format. The body of the fish was constructed using the 2D drawing shown in Figure 11. Based on the Rostrum size, the dimensions of the fish body were derived (Hoover 2013). Then, Gridgen was used to create the fish body. All the parts were imported in Abaqus and used to create the whole fish body.

The structure model (Figure 11) has 10802 linear tetrahedral elements and 2805 nodes. The total number of variables in the structure model is 8415. Computations are carried out only for the Rostrum part (Figure 11). The body of the fish is set up as Display body. The Rostrum and fish body are attached using tie constraints and velocity boundary conditions are applied. Three points are selected on the Rostrum surface. The fish body follows these points as the Rostrum moves. Figure 11 shows the fish model used in the simulation. Figure 12 shows the dimensions of the Rostrum used for the

structure model. Figure 13 shows the guidelines used (Hoover 2013) to measure the dimensions of the Paddlefish. Figure 13, along with the experimental data sheet, provided by Hoover (2013) in Figure 14, which gives guidelines on the size and shape of Paddlefish as a reference to construct the body, fins, and tail of the Paddlefish used in the current simulations.

Figure 11. Fish body used in CSM.

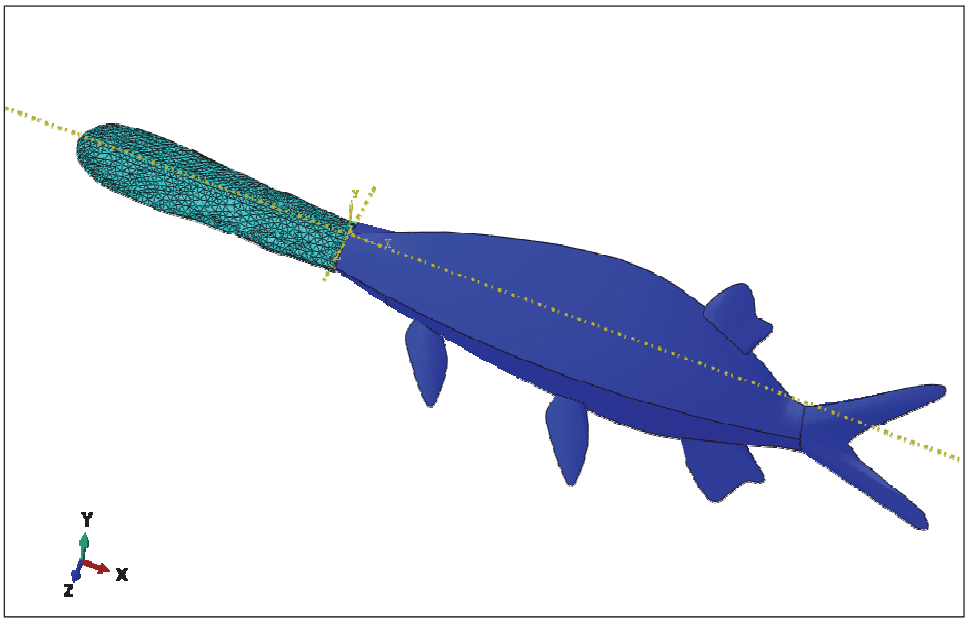

Figure 12. Rostrum dimensions.

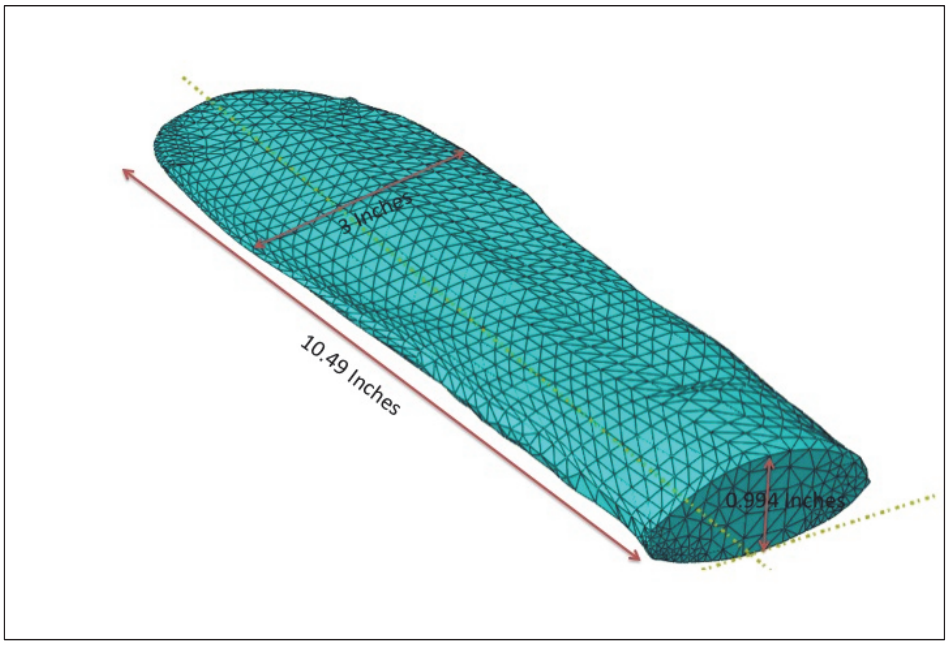

Figure 13. Rostrum structure model dimensions by Hoover (2013).

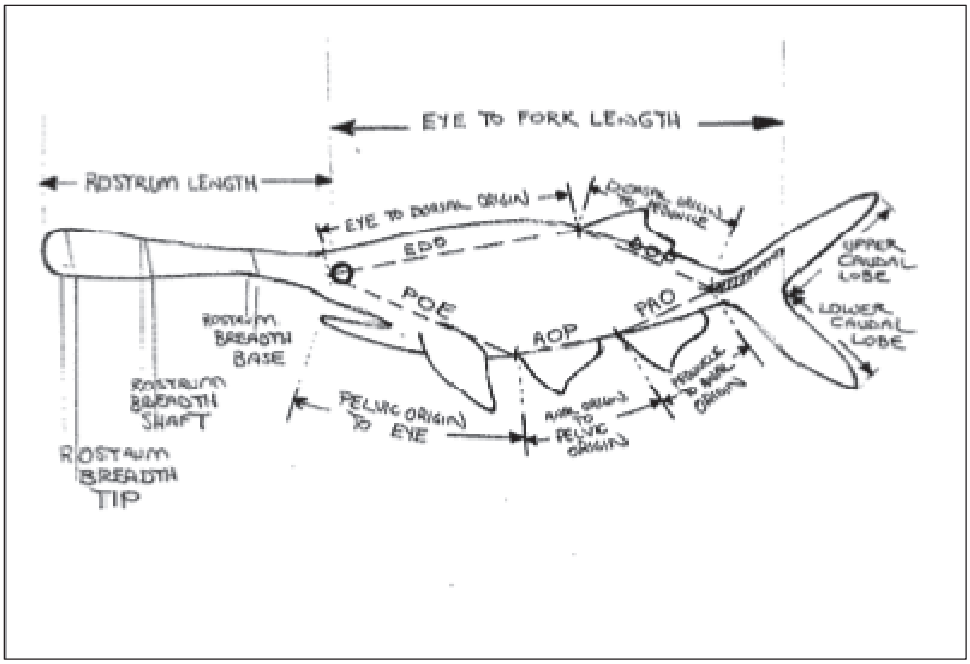

Figure 14. Rostrum structure model dimensions by Hoover (2013).

SPEC_NUMB	ROSTRUM_LENGTH_EFL	WEIGHT (KG)	FINENESS	ROSTRUM_WIDTH_TIP	ROSTRUM_WIDTH_SHAFT	ROSTRUM_WIDTH_BASE
138	227	379	0.73	4.98094	36.69	58.21	58.03
110	232	374	0.87	4.46887	41.33	46.99	57.14
135	234	417	1.05	4.62562	39.54	47.55	65.68
169	237	415	1.34	4.3099	44.41	55.83	61.51
137	241	416	1.05	4.52912	46.6	51.77	58.33
15	283	504	1.41	6.3	52	63	69
6	288	502	0.14	5.51648	48	59	68
8	291	627	2.73	5.31356	56	69	78
4	300	897	7.96	5.67722	80	69	93
7	312	976	9.86	5.6092	83	81	98
12	326	644	3.6	5.152	64	66	86
11	339	955	8.8	5.75301	82	66	87

4 FSI Results

Time dependent fully coupled fluid structure interaction simulations are carried out in the present study to analyze the hydrodynamic and structural properties of Rostrum of the Paddlefish. For implementing these fully coupled simulations, an incompressible fluid solver is used to computationally solve the laminar flow around the entire fish. The fluid solver is coupled with the structural response of the Rostrum in the explicit structure solver. These simulations include the effect of shear forces on the Rostrum and also encompass the effect of deformation of Rostrum on the fluid flow. The deformation of the Rostrum changes the boundary condition of the fluid flow. The interface boundary is explicitly defined during the mesh-making phase.

4.1 Test Case Details

Six FSI simulations are carried out in the present study. The description of the flow parameters and angle of attack used for the test cases is shown in Table 3. Three angles of attack and two activities of swimming fish are analyzed. Three parametric analyses are carried out with fish moving in the direction of fluid flow and three with fish moving against the direction of fluid flow. Very low velocities are used for the investigation to validate the model. Further research in the area will involve additional parametric analyses with varying velocities of water as well as the fish to study the hydrodynamic and structural response of the Rostrum to the fluid flow.

Table 3. Test Case Velocities.

Activity	0 Degree (in/sec)	5 Degree (in/sec)	10 Degree (in/sec)
Fish swimming with the fluid flow (2.5 in/sec)	*Vx* = 2.75 *Vy* = 0	*Vx* = 2.739 *Vy* = 0.2397	*Vx* = 2.70822 *Vy* = 0.4775
Fish swimming against fluid flow (2.5 in/sec)	*Vx* = 2.75 *Vy* = 0	*Vx* = 2.739 *Vy* = 0.2397	*Vx* = 2.70822 *Vy* = 0.4775

4.2 Simulation time and HPC information

All simulations were carried out on HPC-Diamond (SGI Altix ICE 8200). Two nodes were used and a total of 10 cores; 8 cores for CFD and 2 cores for CSM solver. It took an average of 1-hour wall time to simulate 0.1 sec real time. All the test cases were executed for a 7-hour wall time. One

extended simulation was run for 90 hours to ensure that the test cases were run long enough to capture the effects of the flow around the fish and to ensure that the flow disturbance induced by the fish geometry reached a stable flow pattern. In the extended run, changes around the body of the fish after 0.5 sec of real time were not observed. Figure 15 shows the picture of the SGI Altix ICE 8200 (Diamond) located at the ERDC DSRC.

Figure 15. Diamond. SGI ALtix Ice – 172 TFLOPS.

4.3 Velocity profile for fish swimming against the flow direction

Figure 16 shows the velocity profile for fish moving against the direction of flow. The angle of attack used for this execution is zero degrees. The fish is moving in an opposite direction of the fluid flow. When the forward moving Rostrum velocity comes in contact with the opposite flow direction velocity vectors; tiny vortices are created near the top and bottom surface of the Rostrum. The opposite direction of velocity vectors creates these vortices. A high velocity region is seen very close to the upper and lower surface of the Rostrum as seen in Figure 16. At some distance from the Rostrum the magnitude of velocity vectors reaches zero. The zero velocity cloud is seen at this point as seen in Figure 16. After the zero velocity cloud, the velocity increases steadily until it matches the flow velocity. The velocity distribution above and below the surface of Rostrum looks symmetric for angle of attack of zero degree as seen in Figure 16.

Figure 17 depicts the velocity profile for fish moving against the direction of flow. The angle of attack used for this run is 5 degrees. A slight increase in

velocity is seen near the tip of the Rostrum. As seen in Figure 17, an uneven velocity distribution is caused at the tip of the Rostrum when the angle of attack is not zero. This helps propel the fish in upward forward direction.

Figure 16. Velocity profile for fish moving against the flow direction at an angle of attack of 0 degrees.

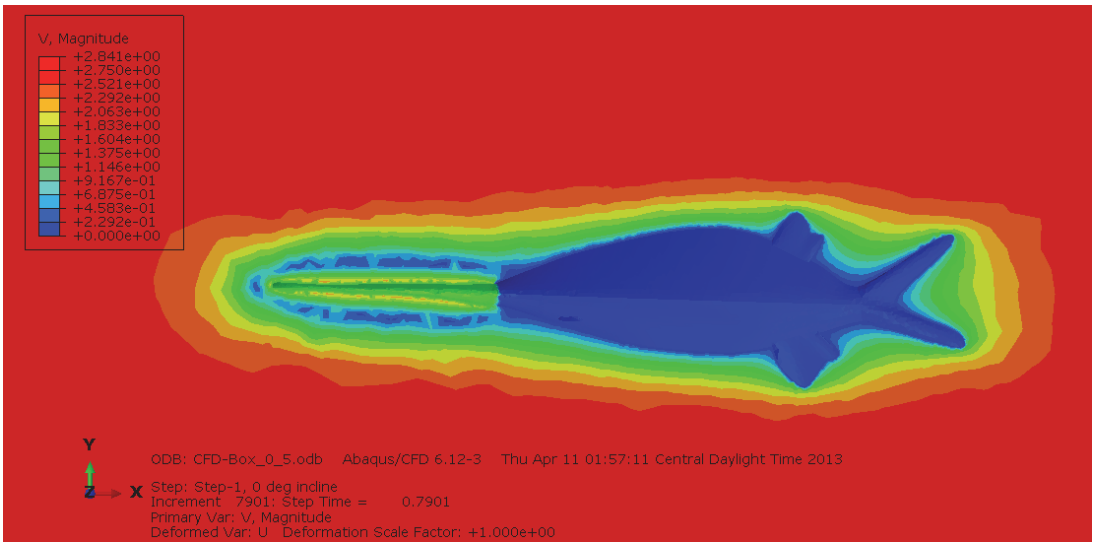

Figure 17. Velocity profile for fish moving against the flow direction at an angle of attack of 5 degrees.

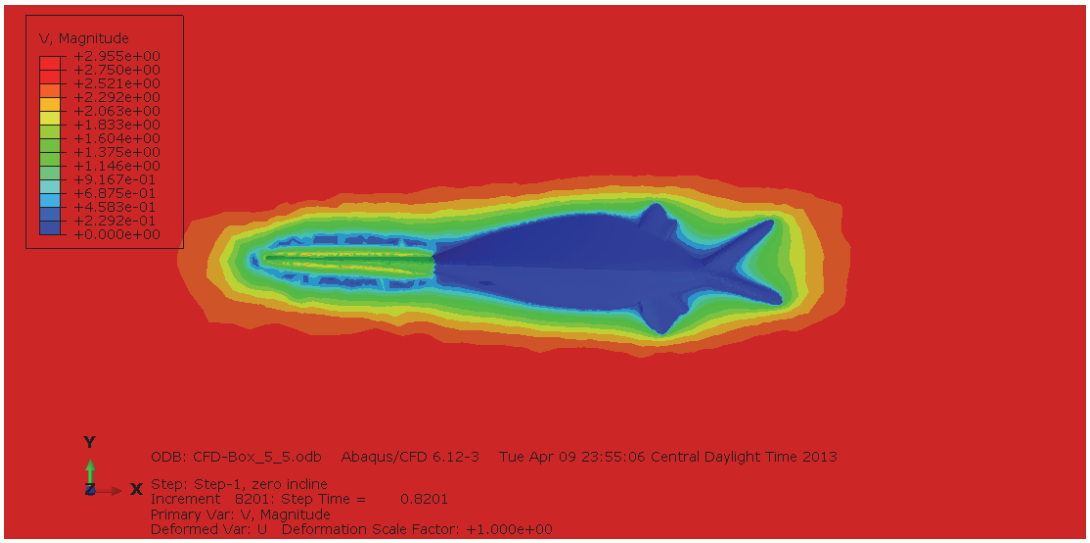

Figure 18 demonstrates the velocity profile for fish moving against the direction of flow for an angle of attack of 10 degrees. An uneven distribution of velocity is observed at the tip of the Rostrum. A similar observation, like that of Figure 17, is seen for the angle of attack of 10 degrees. The increase in velocity at the Rostrum tip is more pronounced as expected.

Figure 18. Velocity profile for fish moving against the flow direction at an angle of attack of 10 degrees.

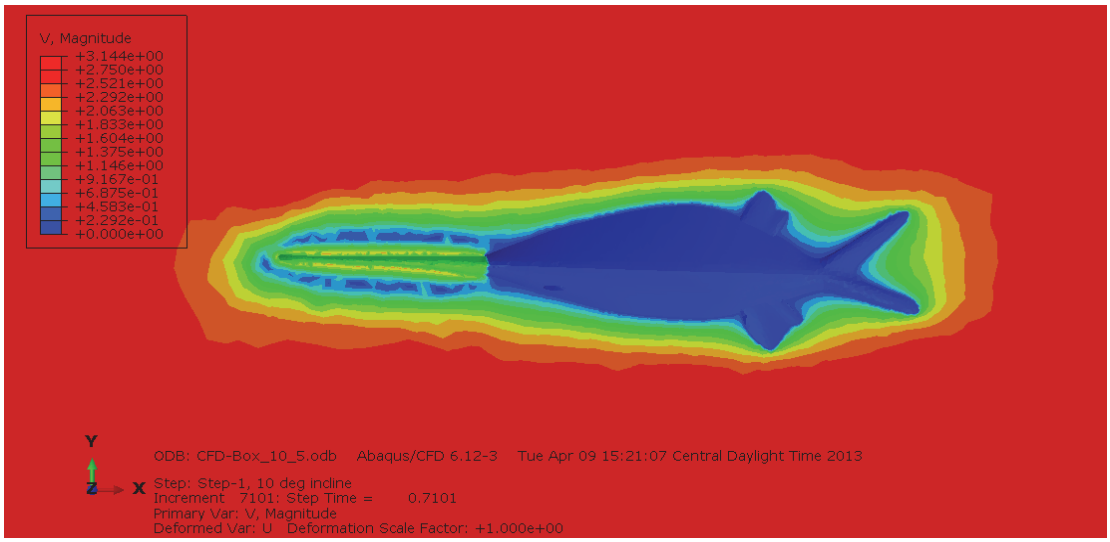

Figures 16 through 18 are the velocity distribution profile at the last time step of the 7-hour simulations. The velocity was stabilized after 0.5 seconds of simulation time. The velocity distribution at the tip of the Rostrum becomes uneven with the increase in angle of attack.

4.4 Velocity profile for fish swimming along the flow direction

When the fish is moving along the longitudinal axis of the flow direction, the flow does not offer much resistance to the movement of the fish. Figure 19 shows the velocity profile for zero angle of attack. Very uniform velocity distribution is observed above and below the Rostrum. The velocity increases as a function of distance as we move away from the body of the fish until it matches the flow velocity as expected.

Figure 19. Velocity profile for fish moving along the flow direction at an angle of attack of 0 degrees.

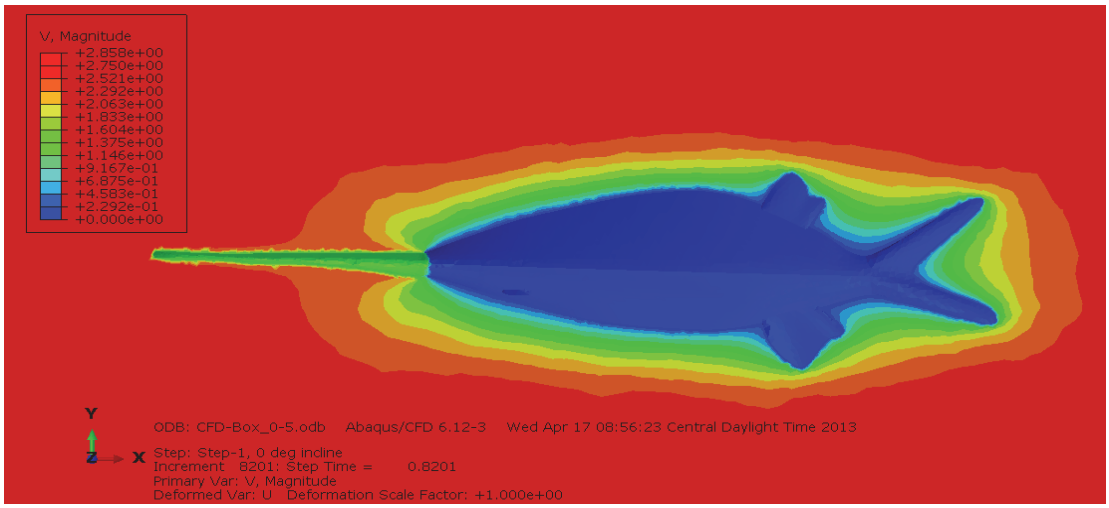

Figure 20 depicts the velocity distribution when the angle of attack of the inflow is 5 degrees. A slight difference in velocity is seen above and below the surface of Rostrum. Velocity increases, as a function of distance, as we move away from the body of fish.

Figure 20. Velocity profile for fish moving along the flow direction at an angle of attack of 5 degrees.

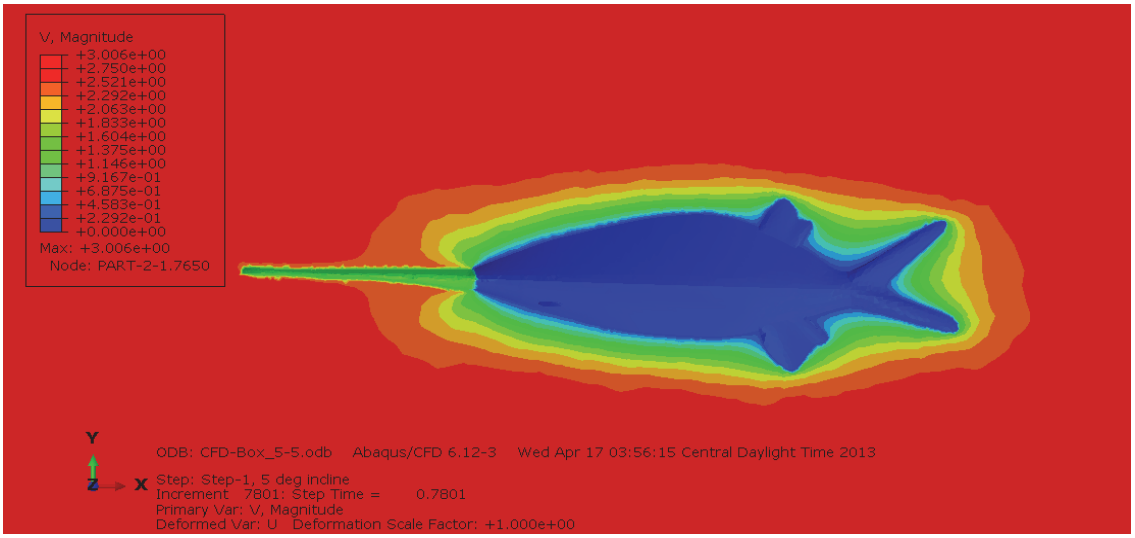

Figure 21 shows the velocity profile when the angle of attack is 10 degrees. An uneven distribution of velocity is observed at the tip of Rostrum as expected.

Figure 21. Velocity profile for fish moving along the flow direction at an angle of attack of 10 degrees.

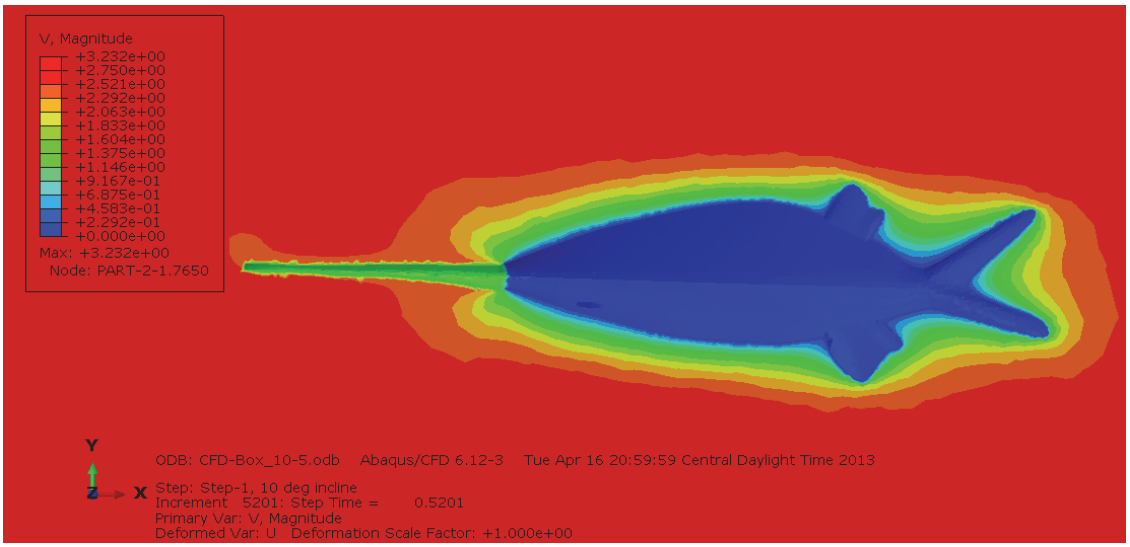

Figures 19 through 21 are the velocity profile at the last time step of the 7-hour simulations.

4.5 Pressure profile for fish swimming against the flow direction

From the basic governing laws of physics, everything in nature has a tendency to evolve to a state where survival is possible with the least possible expenditure of energy. Fish are good examples of this process. The body of a fish is streamlined so that it experiences minimum stresses and also dissipates energy efficiently. In the present study, we have studied the pressure distribution above and below the surface of Rostrum.

Figure 22 shows the pressure contours when the fish is moving against the flow direction. The angle of attack is zero degrees. A high-pressure contour of the order of magnitude 10^{-3} is seen near the tip of the Rostrum. This high-pressure contour is a result of the reaction force between the fluid and fish moving in opposite directions. A small high-pressure bubble is seen near the mouth of the fish. This high-pressure bubble will help push the fish upwards and assist in swimming. High pressures are also seen when the flow comes in contact with the fins and tails as seen in Figure 22.

Figure 22. Pressure profile for fish moving against the flow direction at an angle of attack of 0 degrees.

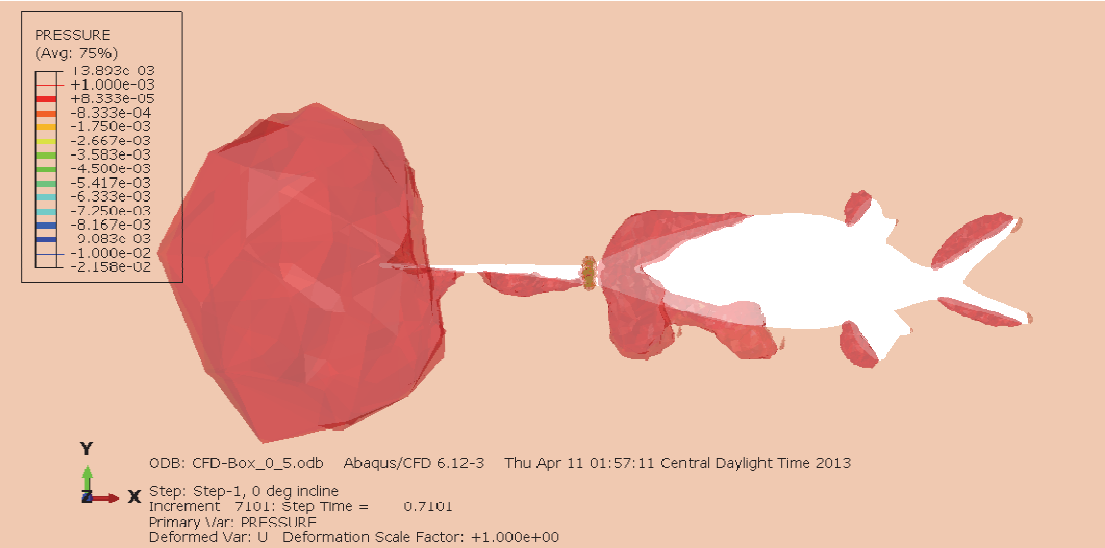

Figure 23 represents the pressure contours when the fish is moving against the direction of flow. The angle of attack is 5 degrees. The angle of attack generates high-pressure on the bottom of the Rostrum of the order of magnitude 10^{-3}. Paddlefish swim with their mouth wide open during filter feeding. They take in enormous amounts of water during this process and transport this water out at a very high velocity. The forward body velocity is used to transport this water. The shape, size, and position of Rostrum generate lift, which assists the fish during this process and also prevents nose-diving.

Figure 23. Pressure profile for fish moving against the flow direction at an angle of attack of 5 degrees.

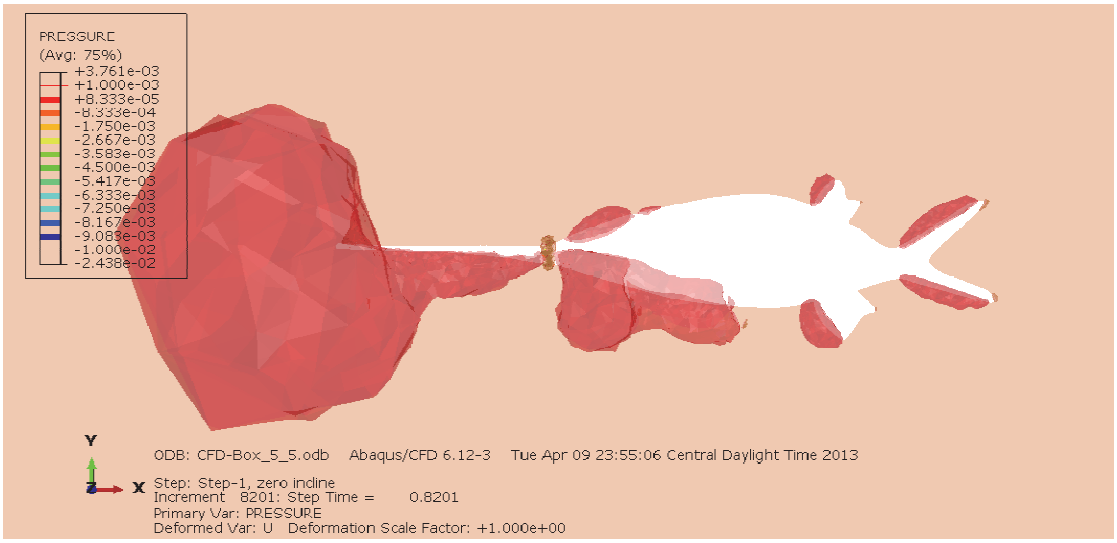

Figure 24 depicts the pressure contours when the fish is moving against the direction of flow. The angle of attack is 10 degrees. Figure 24 shows the negative pressure pocket generated near the mouth of the fish. This negative pressure helps in creating the vacuum that helps the fish gulp in water quickly. High-pressure contours are seen at the bottom of the Rostrum.

Figure 24. Pressure profile for fish moving against the flow direction at an angle of attack of 10 degrees.

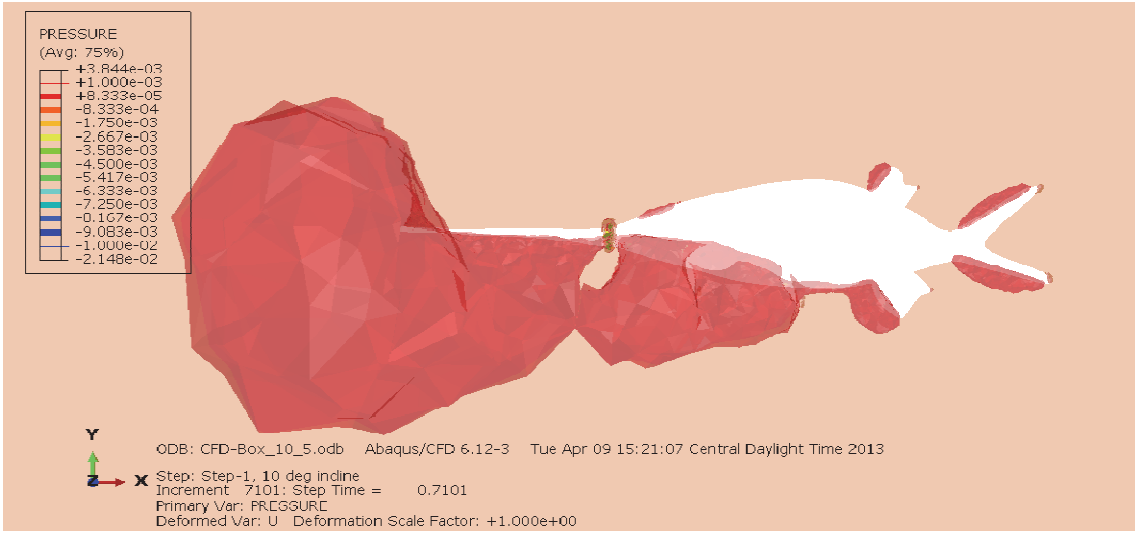

As seen in Figures 22 through 24, the magnitude of the high-pressure is around the same range for all angles of attack. However, when the angle of attack is zero degrees, high-pressure contour is seen at the tip and mouth of the fish. The bottom middle section of the Rostrum area does not experience the high-pressure. When the angle of attack is 5 degrees, the

high-pressure contour covers the entire bottom area of the Rostrum and is more pronounced on the lower body area of the fish. Figure 24 shows that when the angle of attack is 10 degrees, the high-pressure contour covers wider areas on the bottom surface of the Rostrum. Also, the mouth of the fish has a small negative pressure pocket.

4.6 Pressure profile for fish swimming along the flow direction

Pressure contours are created for the simulations when the fish is moving in the direction of flow for the three angles of attack. Since the fish is moving in the direction of the flow, very low resistance is offered by the flow to the movement of the fish. Hence, the reaction force and pressures on the Rostrum are negligible.

Figure 25 shows the pressure contours when the fish is moving in the direction of the flow at an angle of attack of zero degrees. Since the fish is moving in the direction of the fluid flow, the fluid pushes the fish in the forward direction. This will generate high-pressure near the tail and back of fins as seen in Figure 25.

Figure 25. Pressure profile for fish moving along the flow direction at an angle of attack of 0 degrees.

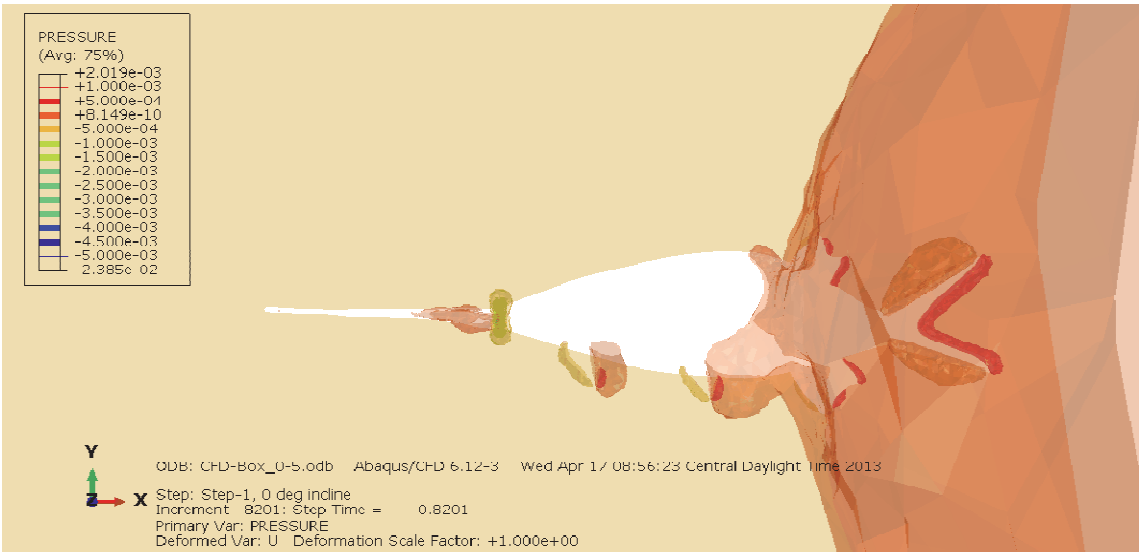

Figure 26 depicts the pressure profile when the fish is moving in the direction of the flow at an angle of attack of 5 degrees. A high-pressure region is seen below the Rostrum. The angle of attack coupled with the shape, size, and position of the Rostrum helps create this high-pressure region.

Figure 26. Pressure profile for fish moving along the flow direction at an angle of attack of 5 degrees.

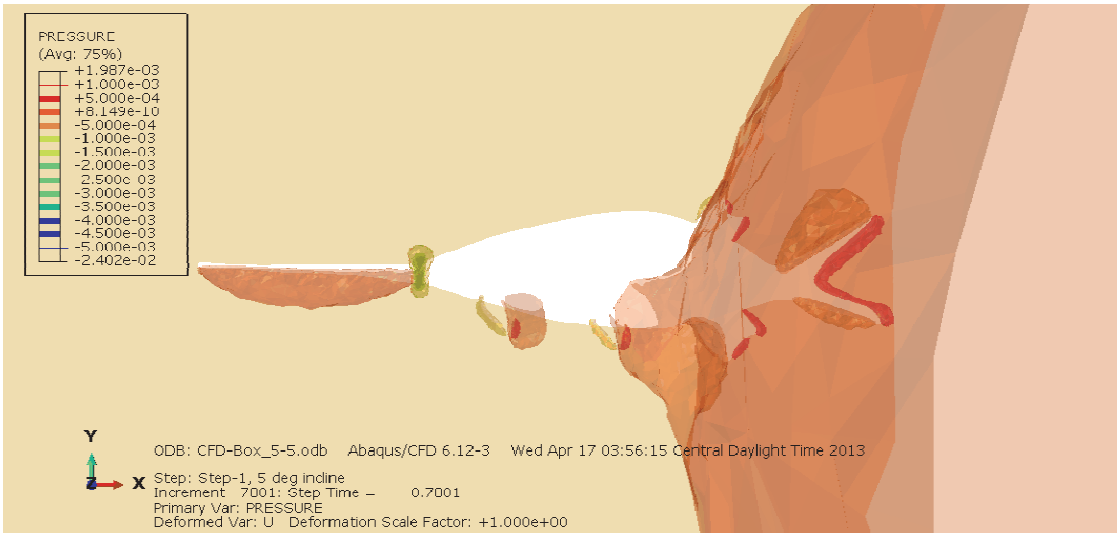

Figure 27 represents the pressure distribution when the fish is moving in the direction of flow at an angle of attack of 10 degrees. The increase in angle of attack makes the high-pressure region below the Rostrum surface more pronounced. High-pressure regions below the surface of Rostrum helps the fish swim efficiently during filter feeding. The size, shape, and position of the Rostrum help stabilize the fish.

Figure 27. Pressure profile for fish moving along the flow direction at an angle of attack of 10 degrees.

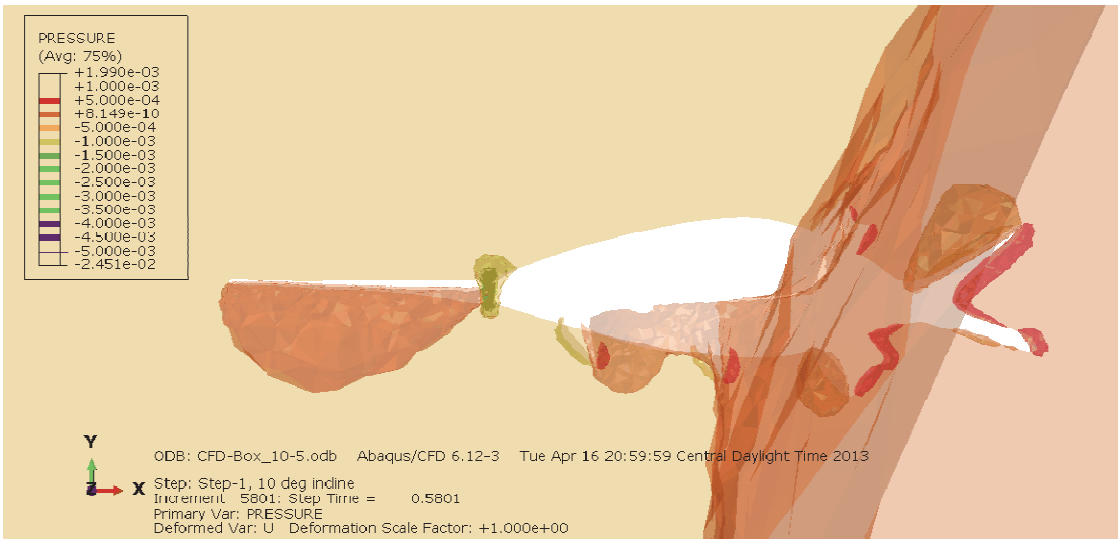

Figures 25 through 27 show the high-pressure contours are the same magnitude (10^{-10}) for the three angles of attack. However, with the increase in angle of attack they spread to larger areas below the Rostrum of the

Paddlefish. Also, since the flow is pushing the fish from behind, higher pressures of magnitude (10^{-4}) are seen at the tail and back of fins.

4.7 Pressure graph near mouth of fish for the three angles of attack

A reference point was picked near the mouth of the fish as seen in Figure 29. Pressure was plotted as a function of time for the three angles of attack. For all three cases, the fish was moving against the direction of flow. Negative pressure peaks are observed when the fish is moving at an angle of attack of ten degrees (Figure 28). These negative pressure peaks help in the filter feeding process. Since these peaks are generated near the mouth of the fish, they help in creating vacuum near the mouth of the fish, which in turn assists in the filter feeding process (Sanderson et al. 1994).

4.8 Pressure on fins of the Paddlefish

Figure 30 shows the pressure on the four fins. For fins 1 and 2, the pressure is positive at the beginning of the simulation as seen in Figure 31. For fins 3 and 4, the pressure is negative at the beginning of the simulation as seen in Figure 32. The overall pressure distribution follows the same trend for all the fins. This is the test case where the fish is swimming against the flow direction. The angle of attack is 10 degrees. Negative pressure peaks are also observed as seen in Figures 31 and 32.

Figure 28. Pressure near the mouth of fish for the three angles of attack.

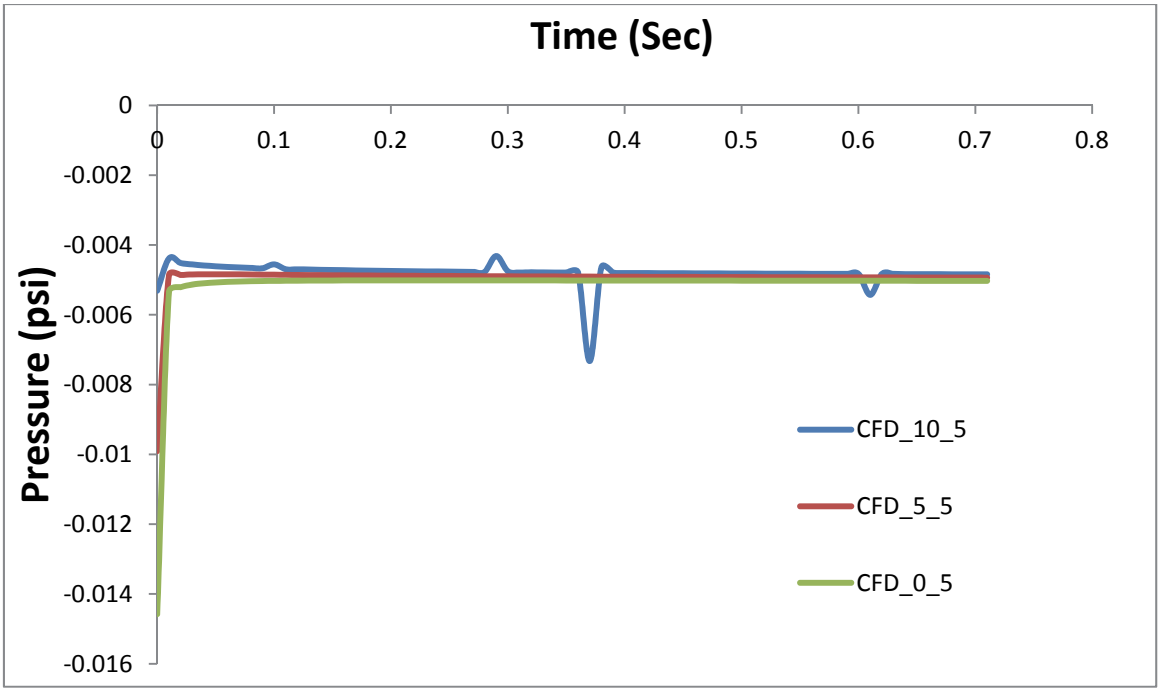

Figure 29. Pressure reference point near the mouth of fish for the three angles of attack.

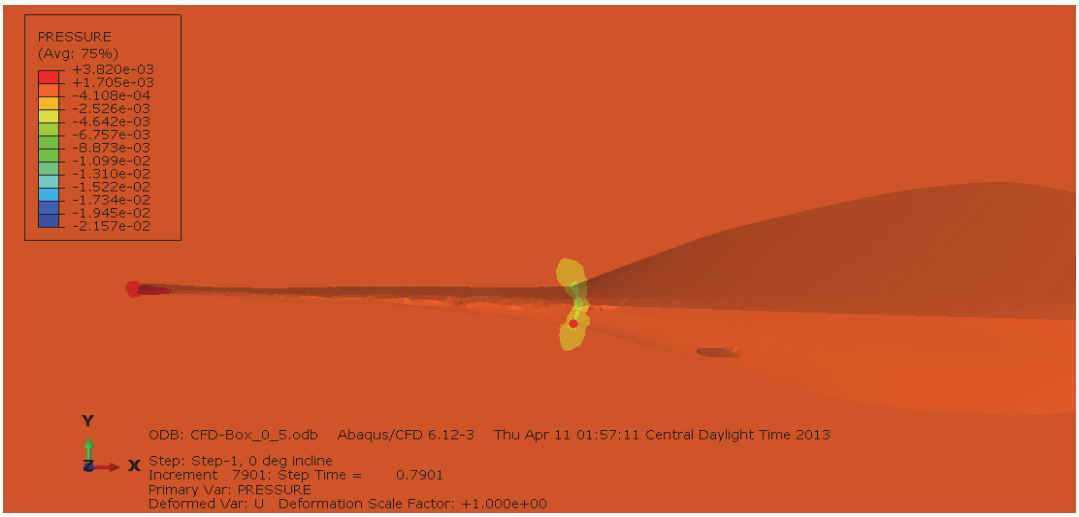

Figure 30. Reference point on fins 1, 2, 3, and 4.

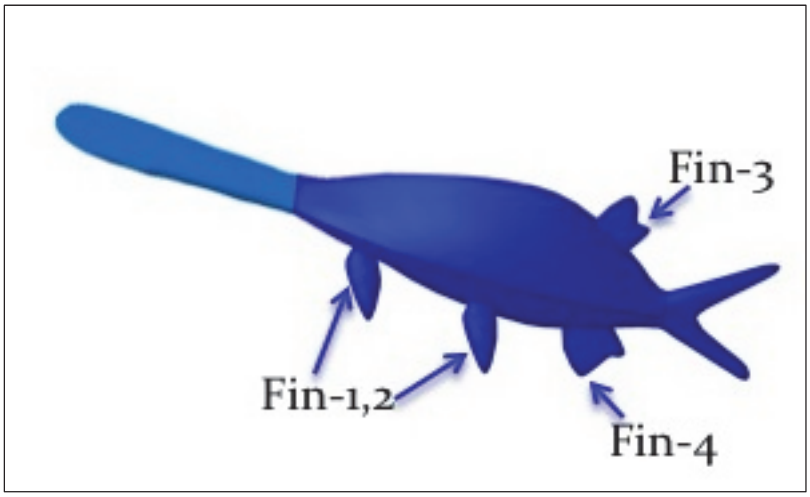

4.9 Pressure graph on bottom/top surface of Rostrum

Pressure is plotted as a function of true distance along path on the top and bottom surface of the Rostrum (Figure 33 and Figure 34). Pressure is plotted as a function of distance for the case in which the fish is moving in the direction of flow for the three angles of attack 0, 5, and 10 degrees. As seen in Figures 35-37, very low pressures are seen on the top and bottom surface of the Rostrum. Also, the pressures on top are slightly lower as compared to the bottom of the Rostrum. As seen in Figure 35, when the angle of attack is zero degrees, the pressure on top and bottom surface are almost identical. As the angle of attack increases, we see higher pressure being developed on the bottom surface of the Rostrum. These higher pressures provide lift, which in turn propels the fish in upward direction and also prevents nose-diving to bottom during filter feeding.

Figure 31. Pressure on fins 1 and 2.

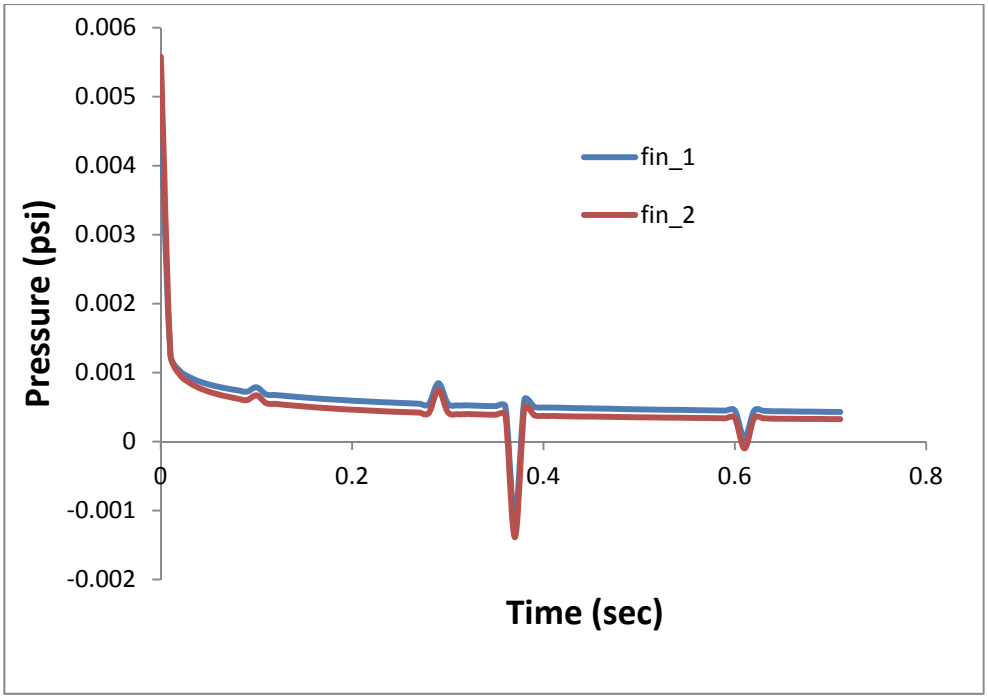

Figure 32. Pressure on fins 3 and 4.

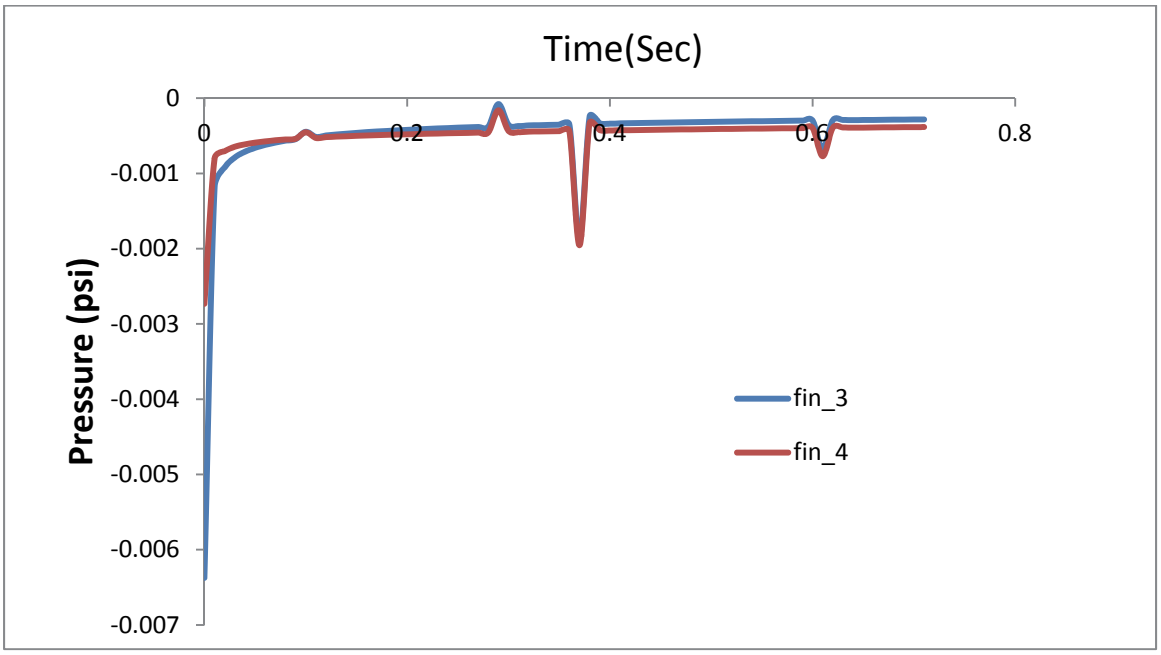

Figure 33. Path reference on Rostrum top.

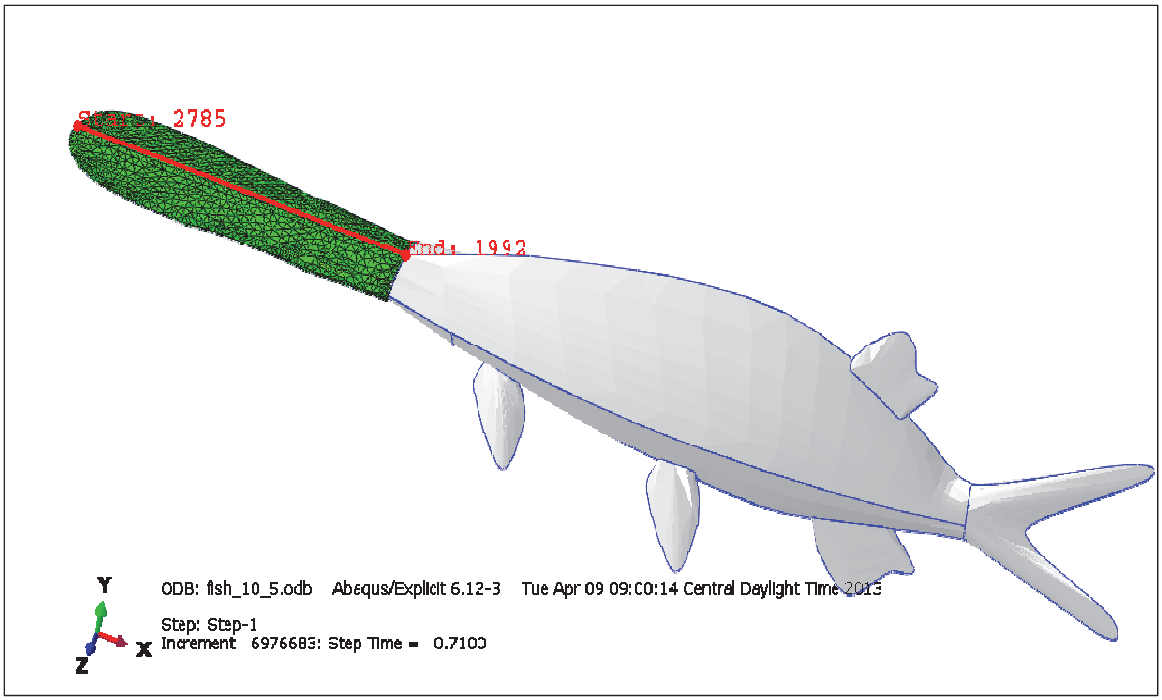

Figure 34. Path reference on Rostrum bottom.

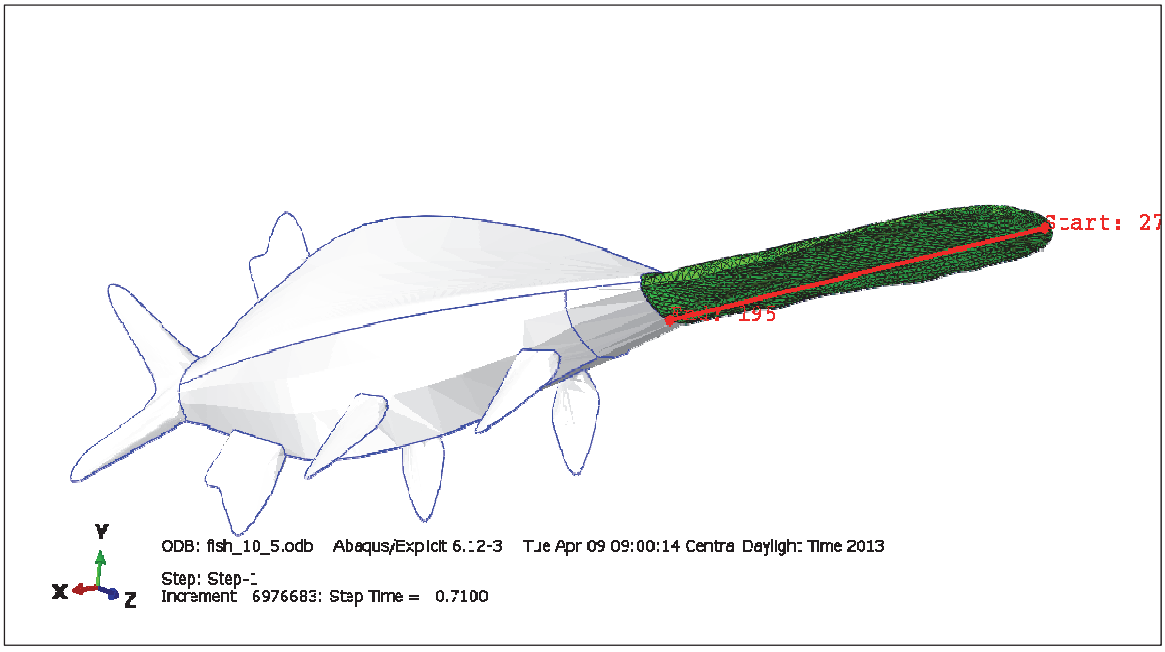

Figure 35. Pressure as a function of true distance on Rostrum top & bottom at an angle of attack of 10 degrees.

Figure 36. Pressure as a function of true distance on Rostrum top & bottom at an angle of attack of 5 degrees.

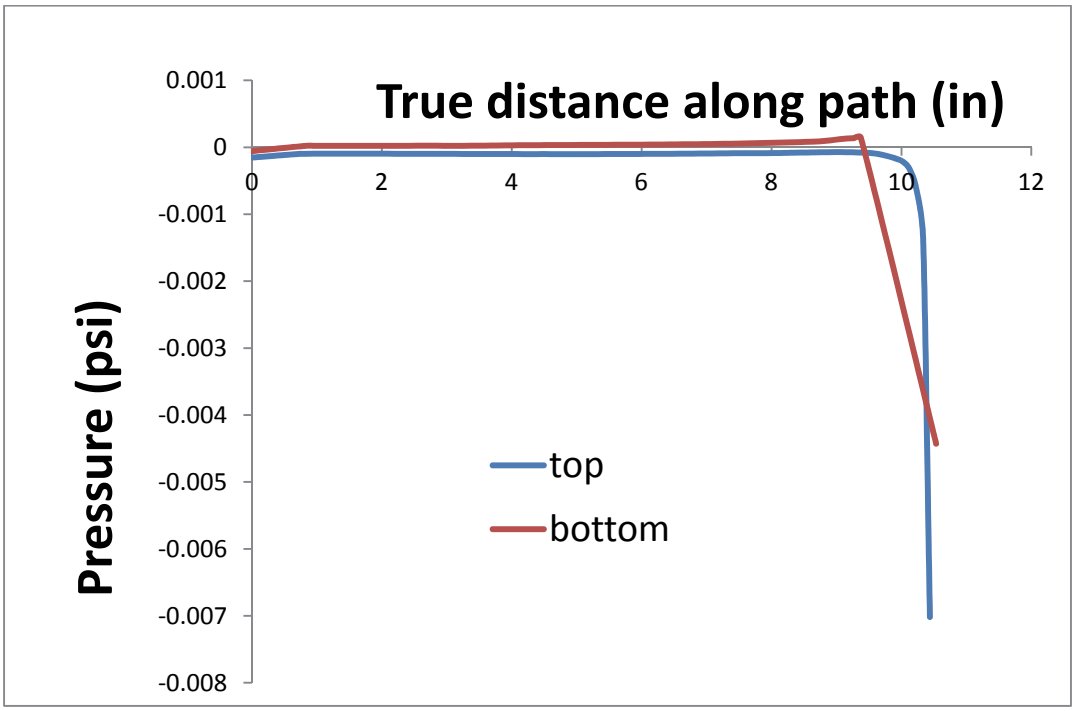

Figure 37. Pressure as a function of true distance on Rostrum top & bottom at an angle of attack of 0 degrees.

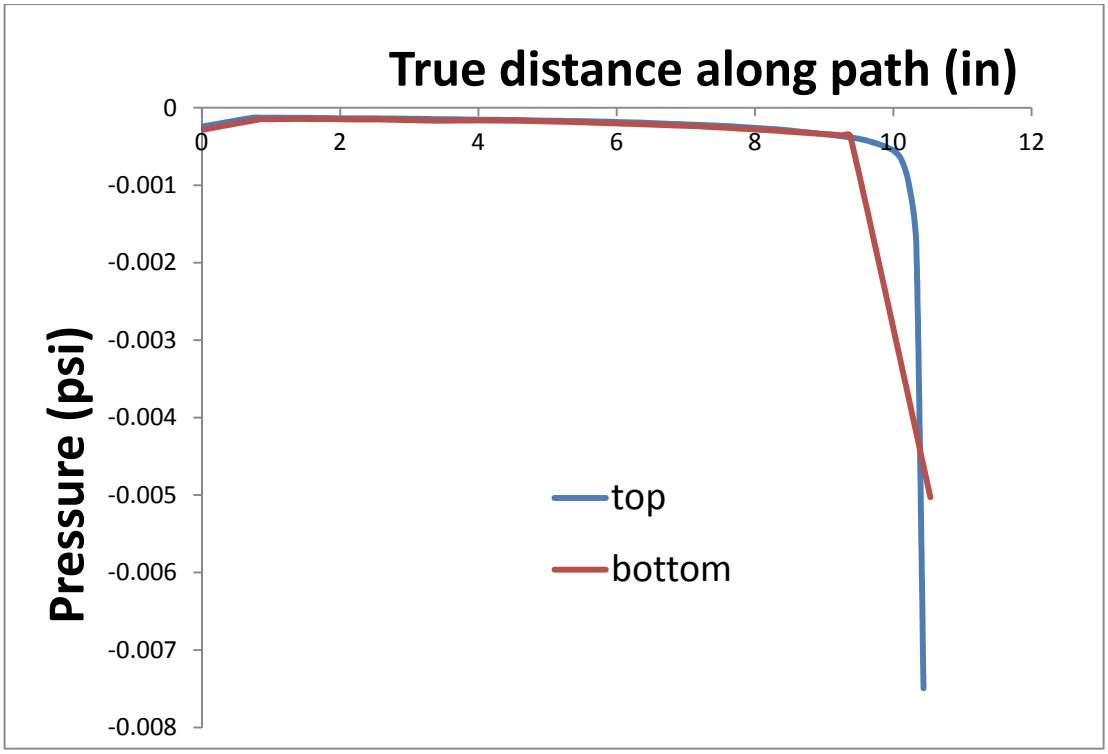

4.10 Velocity graph at Rostrum tip (1)

An uneven distribution of velocity is seen at the top and bottom surface of the Rostrum with the increase in the angle of attack. This effect is more evident at the tip of the Rostrum. Velocity is plotted as a function of time to see the effect of the angle of attack on the velocities. Figure 38 shows the reference point that was picked near the tip of the Rostrum. Velocity is plotted as a function of time for the case when the fish is moving against the flow at the three angles of attack. As seen in Figure 39, with the increase in angle of attack, the velocity at the reference point increases. The angle of attack creates high pressure on the bottom of the Rostrum as seen from the pressure contour plots. The high-pressure on the bottom of Rostrum pushes the fish in an upward direction. This effect coupled with the body velocity of the fish is responsible for the increase in the velocity at the Rostrum reference point shown in Figure 38.

4.11 Velocity graph at Rostrum tip (2)

Another point was picked at the tip of the Rostrum to analyze the increase in velocity with the increase in angle of attack. The reference point shown in Figure 38 is chosen very close to the tip of the Rostrum. Since there is a lot of dynamics involved at the Rostrum tip, the velocity distribution is

studied at another point as well. This reference point is chosen farther away from the tip of the Rostrum. Figure 40 shows the reference point picked at the tip of the Rostrum. As seen in Figure 41, the velocity at the reference point increases with the increase in angle of attack. The zero velocity cloud is not seen around this point. The lift generated because of the Rostrum and the angle of attack is responsible for the increase in velocity around this point.

Figure 38. Velocity reference point at Rostrum tip (1)

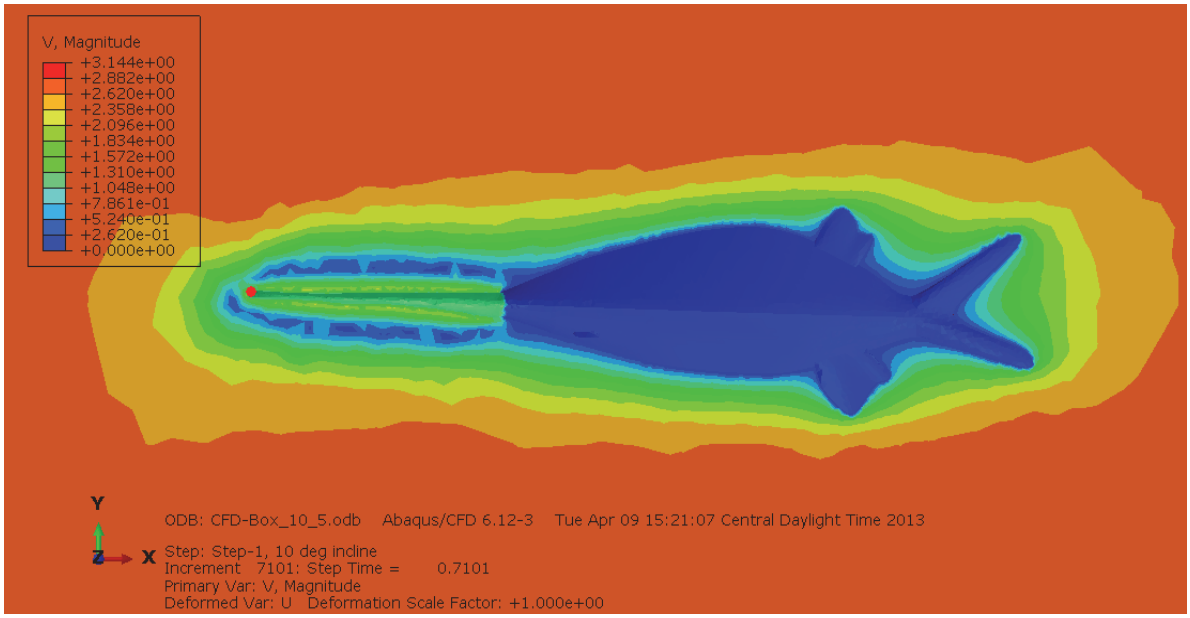

Figure 39. Velocity as a function of time at Rostrum tip (1)

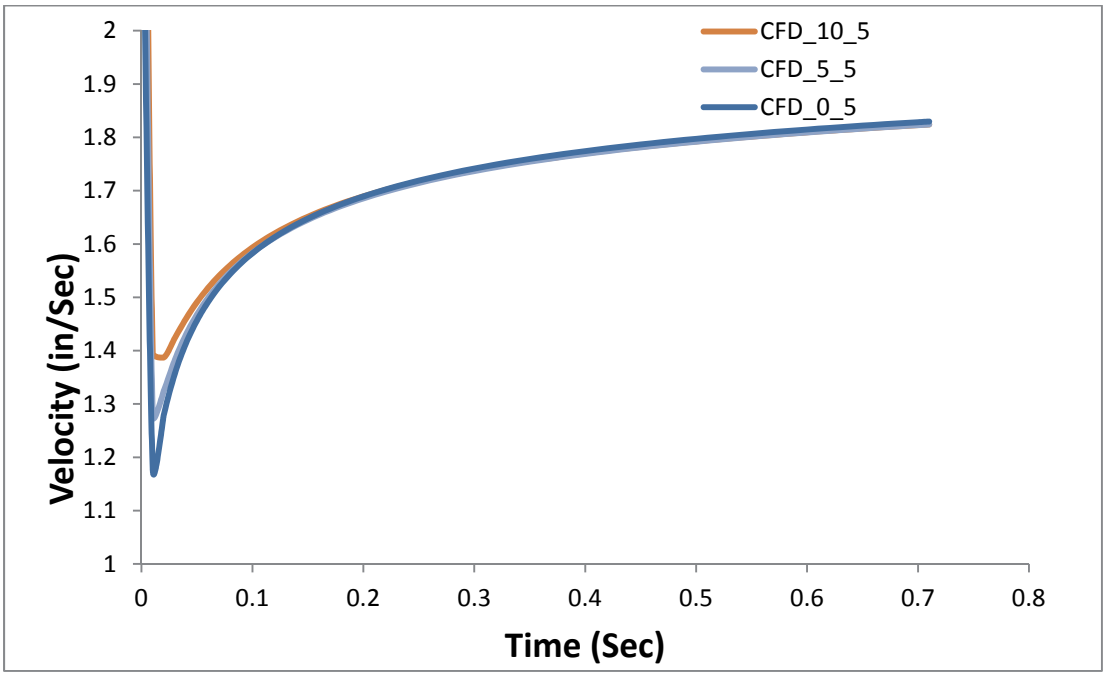

Figure 40. Velocity reference point at Rostrum tip (2)

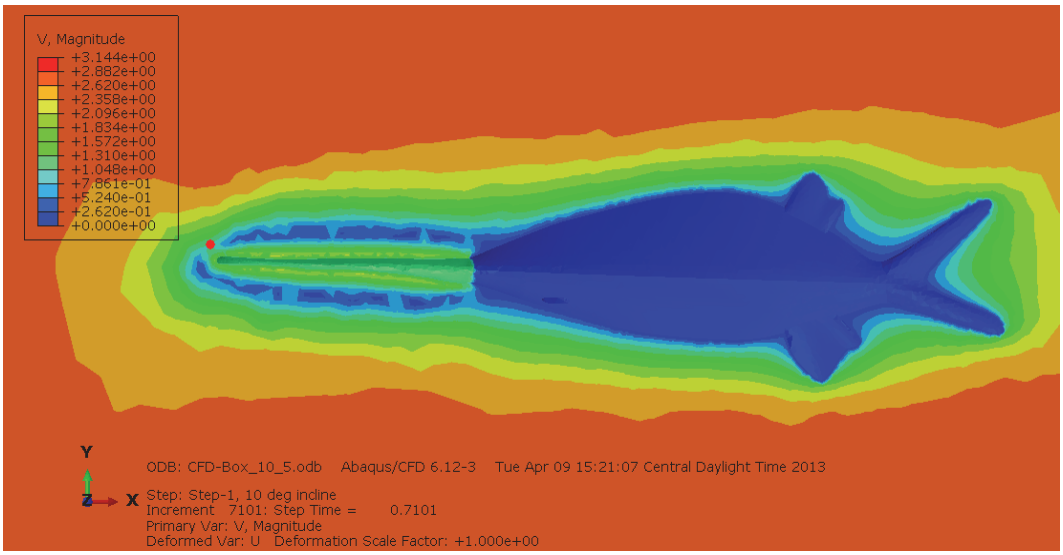

Figure 41. Velocity as a function of time at Rostrum tip (2)

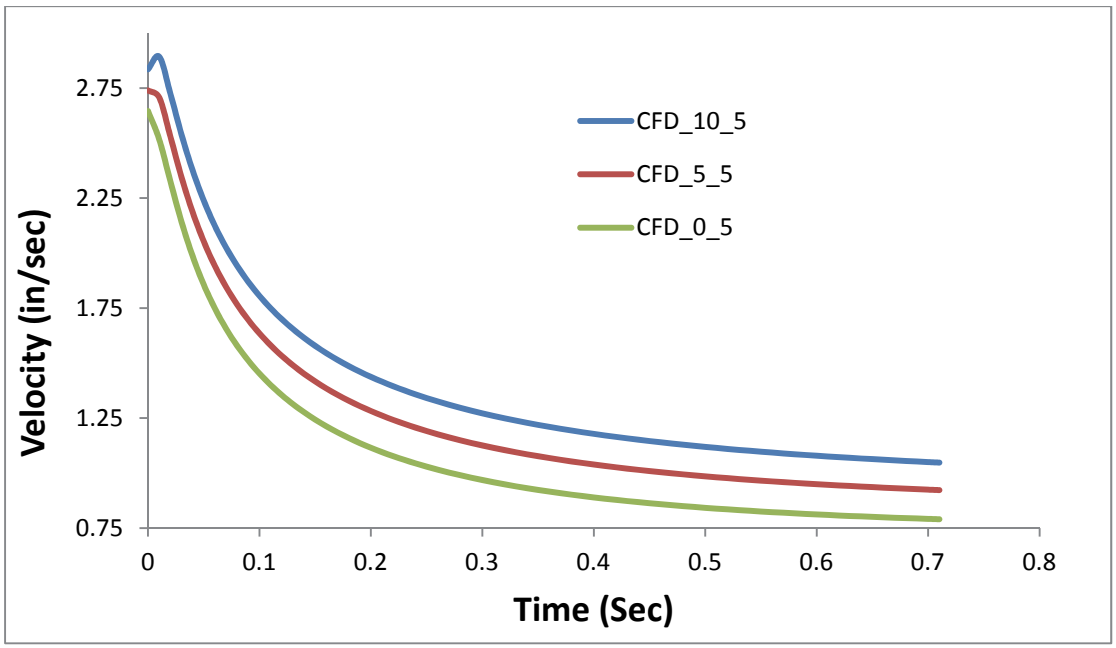

4.12 Streamlines depicting flow patterns

Streamlines help understand and visualize the flow patterns that are not visible to eyes while observing a physical phenomena occurring in nature. When the fish is swimming against the direction of flow, the water particles hit the body of the fish and get reflected in multiple directions creating vortices above and below the Rostrum. Figure 42 shows the flow pattern when the fish is moving against the flow direction. The flow shows a significant amount of disturbance above and below the surface of the Rostrum. As

the flow nears the body of the fish, the vortices and turbulences generated by the paddle begin to dissipate, developing a streamlined flow. Figure 42 also shows how the Rostrum helps stabilize the flow and withstands the disturbance generated when the fish is moving against the direction of flow.

Figure 42. Streamlines when fish is moving against the flow direction

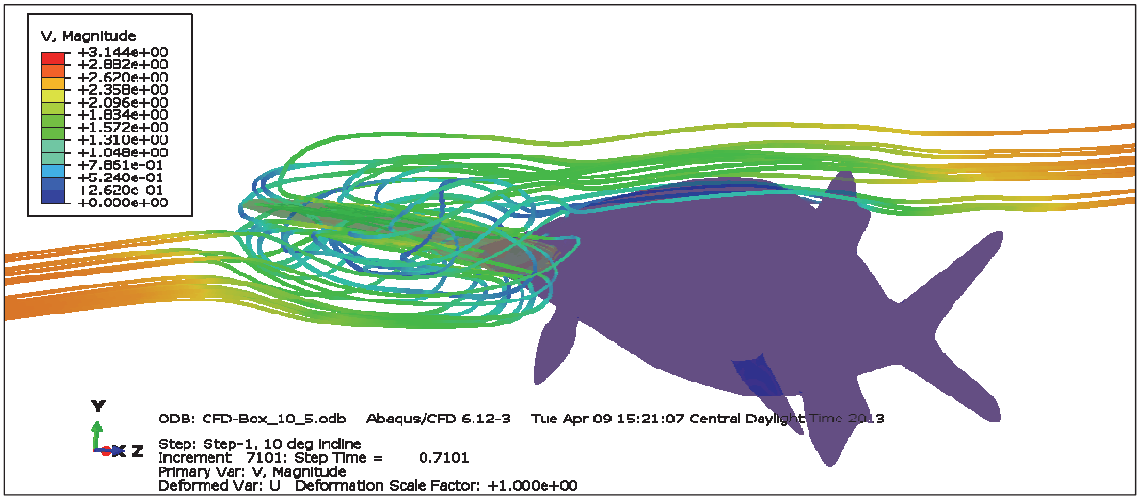

Figure 43 shows the flow pattern when the fish is moving in the direction of flow. The flow is very streamlined and conforms to the body of the fish as visible in Figure 43. No disturbances were seen near the Rostrum. The reaction forces and pressures experienced by the Rostrum in this case are very negligible as discussed in section 4.6 earlier. In this case, the flow of the water helps the fish to propel in forward direction, increasing the velocity of the fish thereby reducing the energy and muscle movement required to swim

Figure 43. Streamlines when fish is moving in the flow direction

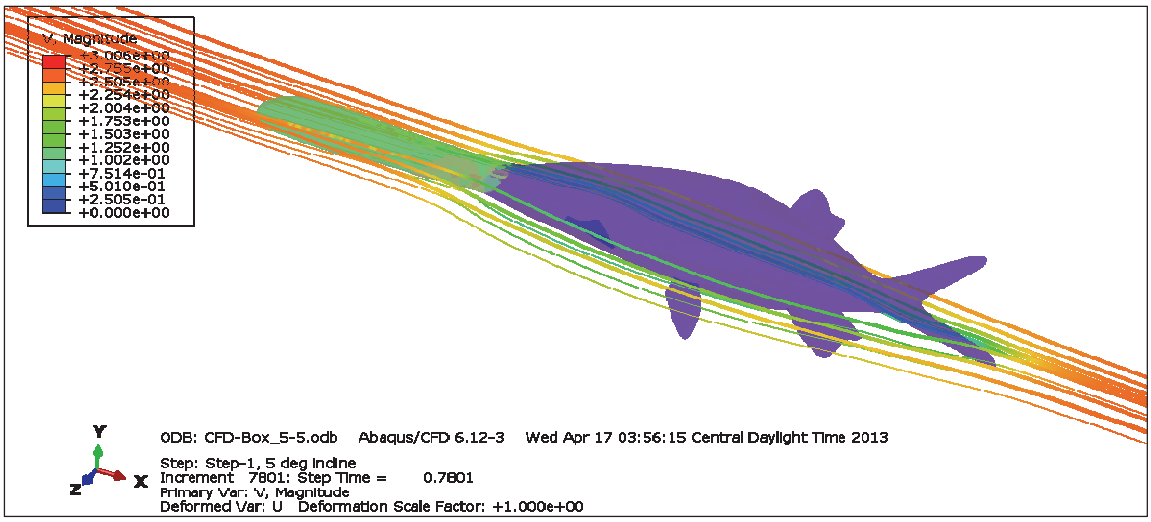

5 Conclusions and Recommendations

5.1 Conclusions

The size, shape, and position of the Rostrum develop the necessary lift required by the fish for filter feeding and balance. During filter feeding, Paddlefish take in enormous amounts of water. This added weight of water would make it extremely difficult for the Paddlefish to swim efficiently. Also, experimental data collected on filter feeding Paddlefish show that they increase their body velocity by ~60 percent to transport this water at very high speeds and filter the tiny zooplanktons from water. To make this process more efficient with minimal amount of muscle activity from the fish, the lift generated by the Rostrum is extremely helpful and required. The lift generated by the presence of Rostrum will reduce the amount of muscle movement required to increase the forward body velocity. Since the shape of the fish is streamlined, the Rostrum as well as the fish body experience very minimum pressures. With the increase in the angle of attack, the pressures on the bottom of the Rostrum increase thereby facilitating the forward movement of the fish just like an aircraft wing.

5.2 Velocity of fish

Based on experimental data collected for Paddlefish kept in round tanks in the laboratory, Paddlefish increase their body velocity by about 60 percent during filter feeding. Fish move by contracting muscles that propel their body in the forward direction. During filter feeding, Paddlefish take in enormous amounts of water in their mouth. Swimming with the added weight of this water will require more effort from the Paddlefish. In addition to this work, there will be the fact that Paddlefish use forward body velocity to transport this water at high velocity. The lift generated by the Rostrum during this phase will tremendously reduce the amount of work required by the fish to move at high speed. Also, when the fish is moving against the flow of water, Rostrum acts as a stabilizer. It forms a zero velocity cloud on top and bottom surface of the Rostrum that takes care of the vortices generated due to the fish body and makes the fluid flow streamlined when it reaches the body of the fish.

5.3 Pressure on Rostrum

The body of fish is streamlined and designed to withstand the static pressure and the pressures generated due to flow around the fish body. Uplift pressures on the Rostrum are generated to aid the fish swim efficiently when the angle of attack increases. In the current study, we have found very low pressures on the surface of the Rostrum. Also, high uplift pressure is generated on the bottom of the Rostrum that helps generate lift. Negative pressure pockets were seen at the angle of attack of 10 degrees. These negative pressure pockets create the vacuum effect that aids the fish in taking in large amounts of water during filter feeding. The mechanical property and shape of the Rostrum is designed such that it dissipates energy efficiently, it is lightweight, withstands pressure load efficiently, and enhances the generation of vortices that develop uplift pressures during filter feeding.

5.4 Angle of attack of Rostrum

The increase in angle of attack of the flow generates higher pressure on the bottom of the Rostrum. These increases in uplift pressures help generate lift that propels the fish in the forward direction. During filter feeding, the fish takes in enormous amount of water and transports this water at very high velocity. Paddlefish uses forward body velocity to transport this water. The lift generated by the Rostrum in conjunction with the angle of attack helps in this process. We have observed that the increase in angle of attack generates negative pressure peaks that aid in filter feeding.

5.5 Recommendations for Further Research

1. Include the hierarchical structure of the Rostrum in the structure model. Although the experimentally measured mechanical properties for Rostrum are used for the structural model, the incorporation and the development of hierarchical structure will throw light towards developing better performing materials.
2. Compare different Reynolds number flows. Since Paddlefish are known to feed in both laminar and turbulent flows, it will be beneficial to see the flow pattern around the fish and the structural properties of Rostrum in turbulent flows.
3. Since the main focus of this study is on the lift generated by the Rostrum during filter feeding, including the mouth opening phenomena during ram filter feeding seems to be the next logical step.

4. The experimental data available for Paddlefish during filter feeding is very limited. Future research needs to concentrate on performing experiments to determine fish swimming patterns and velocities, pressures, angles of attack, Reynolds number of flow, etc.
5. The lack of material data on fish body has led us to include the body of fish as a display body. Future research efforts may be directed towards including the muscle movement of the fish body in the structure model to simulate a more realistic swimming fish.

References

Alexander, M. I. 1914. The Paddle-fish (polyodon spathula). *Trans. Amer. Fish. Soc.,* 44:73-78.

Allen, J. B., and G. A. Riveros. 2013. *Hydrodynamic characterization of the Polyodon Spathula Rostrum using CFP*. In preparation.

Allison, P. G., M. Q. Chandler, R. I. Rodriguez, B. A. Williams, R. D. Moser, C. A. Weiss Jr., A. R. Poda, B. J. Lafferty, A. J. Kennedy, J. M. Seiter, W. D. Hodo, and R. F. Cook. 2013. Mechanical properties and structure of the biological multilayered material system, Atractosteus spatula scales. *Acta Biomaterialia*, 9(2): 5289-5296.

Beach, H. 1902. The Paddlefish, Polyodon Spathula. *Bull. Wis. Nat. Hist. Soc.*, 2:85-86.

Bergmann, M., and A. Iollo. 2010. *Modeling, simulation and control of fish-like swimming*. Bordeaux, France: Institut de Mathématiques de Bordeaux. Computational Dynamics 2010, pp 689-694.

Forbes, S. A. 1878. The food of Illinois fishes. *Bull III. State Lab. Nat. Hist.*, 1: 71-89.

Forbes, S. A. 1888a. *Studies of the food of freshwater fishes*. Ibid., 2: 433-473.

Forbes, S. A. 1888b. *On the food relations of freshwater fishes: A summary and discussion*. Ibid., 2: 475-538.

Gurgens, C., D. F. Russell, and L. A. Wilkens. 2000. Electrosensory avoidance of metal obstacles by the Paddlefish. *Journal of Fish Biology*, 57: 277-290.

Hoover, J., E. Perkins, and P. Allison. 2013. *Structural and material properties of the Paddlefish Rostrum*. In proceedings to Technical Directors, Vicksburg, MS: US Army Engineer Research and Development Center, February 2013.

Hou, G., J. Wang, and A. Layton. 2011. Numerical methods for fluid-structure interaction-A Review: *Commun. Comput. Phys.*

Jennings, C. A., and S. Zigler. 2009. *Biology and life history of Paddlefish in North America: An update*. Pages 1-22 in C. P. Paukert and G. D. Scholten (eds) Paddlefish Management, Propagation, and Conservation in the 21st Century: Building From 20 Years of Research and Management. Bethesda, MD: American Fisheries Society.

Jordan, D. S., and B. W. Evermann. 1896. The fishes of North and Middle America. *Bull. US Natl. Mus.*, 47:I-1240.

Meyer, F. P. 1960. Life history of Marispometra Hastata and the biology of its host, Polyodon Spathula. Unpubl. PhD thesis. Iowa State University. Ames.

Norris, H. W. 1923. On function of the paddle of the Paddlefish. *Proc. Iowa Acad. Sci.* 30:135-137.

Prasad, S., Y. Y. Lu, S. Harwood, K. Mukundakrishnan, and M. Sanchez Rocha. 2011. Co-simulation and multiphysics technologies for coupled fluid-structure interaction problems. Boston, MA: In *Proceedings, NAFEMS World Congress*. April 2011.

Saffron, I. 2002. *Caviar – The strange history and uncertain future of the world's most coveted delicacy*. Broadway Books, New York.

Sanderson, S. L., J. J. Cech, Jr., A. Y. Cheer. 1994. Paddlefish buccal flow velocity during ram suspension feeding and ram ventilation. *J. exp Biology*, 186: 145-156.

Schutte, J. H., J. F. Dannenberg, Y. H. Wijnant, and A. de Boer. 2010. *An implicit and explicit solver for contact problems*.University of Twente. Institute of Mechanics. In Proceedings of ISMA 2010.

Sen, D. 2011. *Improvement in mechanical properties through structural hierarchies in bio-inspired materials*: Dissertation Massachusetts Institute of Technology.

Sprague, J. W. 1959. Report of fisheries investigations during the sixth year of impoundment of Fort Randall Reservoir, South Dakota: South Dakota Dep. Game Fish Parks Dingell-Johnson Project F-I-R-8.

Stockard, C. R. 1907. Observations on the natural history of Polyodon Spathula. *Amer. Nat*. 41: 753-766

Stockard, C. R. 1908. Our new caviar fisheries, *Century Magazine* 76(Series 54), 457-462.

Toro, E. F. 1999. 2nd Edition. *Riemann solvers and numerical methods for fluid dynamics*. A practical Introduction.

Tower, W. S. 1908. The passing of the sturgeon – A case of the unparalleled extermination of a species, *Popular Science Monthly,* 73: 361-371.

Vepari, C. and D. L. Kaplan. 2007. Silk as Biomaterial. *Prog Polym Sci.*, 32(8-9): 991–1007.

Wilkens, L. A., D. F. Russell, X. Pei, and C. Gurgens. 1997. The Paddlefish Rostrum functions as an electrosensory antenna in plankton feeding. *Proc. R. Soc. Lond.*, B 264: 1723-1729.

Wilkens, L. A., and M. H. Hofmann. 2007. The Paddlefish Rostrum as an electrosensory organ: a novel adaptation for plankton feeding. *BioScience,* 57: 399-407.

Williamson, D. F. 2003. *Caviar and conservation – Status, management, and trade of North American sturgeon and Paddlefish*. TRAFFIC North America, Washington, DC: World Wildlife Fund.

REPORT DOCUMENTATION PAGE

Form Approved
OMB No. 0704-0188

1. REPORT DATE *(DD-MM-YYYY)*	2. REPORT TYPE	3. DATES COVERED *(From - To)*
September 2013	Final Report	

4. TITLE AND SUBTITLE

Towards development of Innovative Bio-Inspired materials by analyzing the Hydrodynamic properties of Polyondon Spathula (Paddlefish) Rostrum

5a. CONTRACT NUMBER

5b. GRANT NUMBER

5c. PROGRAM ELEMENT NUMBER

6. AUTHOR(S)

Reena R. Patel and Guillermo A. Riveros

5d. PROJECT NUMBER

5e. TASK NUMBER

5f. WORK UNIT NUMBER

7. PERFORMING ORGANIZATION NAME(S) AND ADDRESS(ES)

Information Technology Laboratory
US Army Engineer Research and Development Center
3909 Halls Ferry Road
Vicksburg, MS 39180-6199

8. PERFORMING ORGANIZATION REPORT NUMBER

ERDC/ITL TR-13-4

9. SPONSORING / MONITORING AGENCY NAME(S) AND ADDRESS(ES)

US Army Corps of Engineers
Washington, DC 20314-1000

10. SPONSOR/MONITOR'S ACRONYM(S)

11. SPONSOR/MONITOR'S REPORT NUMBER(S)

12. DISTRIBUTION / AVAILABILITY STATEMENT

Approved for public release; distribution is unlimited.

13. SUPPLEMENTARY NOTES

14. ABSTRACT

Paddlefish can be distinguished from other freshwater fish by the presence of a long paddle shaped snout (Rostrum). The Rostrum has desirable mechanical characteristics that could be explored to design bio-inspired materials that have better strength to weight ratio. The Rostrum is large and generates lift like an aircraft wing. It acts as a stabilizer preventing drag during filter feeding when the mouth is wide open. This report will discuss the Fluid Structure Interaction simulations conducted to analyze the lift generated by the Rostrum, fluid flow around the fish, pressures on the Rostrum, fluid induced swimming enhancements, and stabilizing properties of the Rostrum. The report analyses and discusses the experimentally measured forward body velocity of Paddlefish during filter feeding. Laminar flow with different angles of attack (0, 5, and 10) along and against the direction of the longitudinal axis of the swimming fish are also studied and discussed.

15. SUBJECT TERMS

Paddlefish
Rostrum
Bio-inspiration
Filter feeders
Multiphysics techniques
Fluid flow
Body velocity
Lift

16. SECURITY CLASSIFICATION OF:			17. LIMITATION OF ABSTRACT	18. NUMBER OF PAGES	19a. NAME OF RESPONSIBLE PERSON
a. REPORT	b. ABSTRACT	c. THIS PAGE			19b. TELEPHONE NUMBER *(include area code)*
unclassified	unclassified	unclassified		49	